Thesis for a Ph.D. degree

Analyzing the sources and influences of groundwater contaminant using direct and indirect data

지하수 오염의 원인과 영향 분석을 위한

직접 및 간접 자료의 활용

Lim, Joung-Won

AUGUST 2013

School of Earth and Environmental Sciences

Graduate School

Seoul National University

Analyzing the sources and influences of groundwater contaminant using direct and indirect data

지도교수 이 강 근

이 논문을 이학박사 학위논문으로 제출함

2013 년 8 월

서울대학교 대학원

지구환경과학부

임 정 원

임정원의 이학박사 학위논문을 인준함

2013 년 8 월

위원장 이 인 성 (인)

부위원장 이 강 근 (인)

위원 김 준 모 (인)

위원 현 윤 정 (인)

위원 김 규 범 (인)

Abstract

Often the groundwater contamination is derived from multiple causes of both the environmental and anthropogenic sources. Thus, analysis of contamination needs to be approached with multiple methods appropriate for the characters of investigation site. This study suggests integration of different methods which are properly chosen according to the site specific characteristics when evaluating groundwater contamination. Each of the three topics which comprise this study deals with analysis of groundwater contamination from environmental-anthropogenic coupled sources in various environment.

In the first topic, modeling of solute transport is integrated into a regression method to analyze the effect of land use on groundwater quality and to predict contaminant concentration of groundwater in an agricultural region. A backward transport equation, which is a mathematical model based on the physical processes of solute transport, is used to delineate probabilistic capture zones. The probabilistic capture zone defines the area where contaminant discharge can have a direct influence, with pertinent probability, on the quality of groundwater pumped from a well. Tobit regression analysis is used to find the relationship between independent regression variables and a dependent variable, which is a contaminant concentration in this study.

The capture zone and the regression analysis are combined into a model, and its applicability for prediction of nitrate concentration is tested in a small agricultural basin in Chuncheon, Korea, which is occupied mainly by vegetation fields, orchards, and small barns.

The second topic is about leachate transport from livestock mortality burial during the decomposition of carcasses. Due to the specificity of the site, there was only one well for monitoring and sampling groundwater and it was difficult to set up additional wells even for research purposes. In order to overcome the limitation of using monitoring wells, electrical resistivity survey is used as an alternative method of obtaining data. The electrical resistivity measures were compared with the result of leachate transport model of the study site. The properties of the images from the two different methods were compared and analyzed for quantitative assessment of the simulation model to increase accuracy in prediction of leachate transport.

The last topic uses hydrogeochemical and isotopic indicators to assess the characteristics of salinized seepage into an underground oil storage cavern in a coastal area of Yeosu, Korea. The construction and operation of underground caverns can act as groundwater sinks near a coastal area. In an environment complicated with such artificial structures, seawater intrusion is not simple and thus needs to be evaluated by

means of multiple analytical approaches. Cl^-/Br^- ratios, principal component analysis (PCA) of chemical data, and stable isotope data were used to determine the origin and the extent of salinization. These data are interpreted under the context of hydrogeological feature of the study area.

Keywords: groundwater quality, modeling, probabilistic capture zone, regression analysis, PCA, ion ratio, stable isotope, electrical resistivity survey, image similarity

Contents

Pages

Abstract i

Contents iv

List of Figures vii

List of Tables xiii

Chapter 1 Introduction 1

Chapter 2 Model-integrated regression analysis of groundwater contamination at an agricultural region 6

2.1 Introduction 8

2.2 Methods 11

2.2.1 Delineating probabilistic capture zone 14

2.2.2 Tobit regression 18

2.2.3 Model-integrated regression analysis 20

2.2.3.1 Site Description 20

2.2.3.2 Application 24

2.3 Results & Discussion 35

2.4 Conclusion 41

Chapter 3 Analysis of leachate transport at a livestock burial site using a model validated with geophysical data 44

3.1 Introduction 46

3.2 Site Description 48

3.3 Methods 53

3.3.1 Electrical resistivity survey 53

3.3.2 Simulation of leachate transport 56

3.3.3 Image similarity metric 62

3.4 Results and Discussion 63

3.4.1 Electrical resistivity near the burial pits 63

3.4.2 Leachate transport from the burial 71

3.4.3 Image similarity: IMED 75

3.5 Conclusion 79

Chapter 4 Hydrogeochemical analysis of salinity in groundwater in a coastal environment 81

4.1 Introduction 83

4.2 Site description 86

4.3 Methods 90

4.3.1 Sampling and analysis 90

4.3.2 Data analysis 94

4.4 Results 96

4.4.1 Na^+, Cl^- and EC 96

4.4.2 Cl^-/Br^- ratio 102

4.4.3 Principal component analysis 105

4.4.4 Stable isotope analysis 110

4.4.5 Cl^--Br^- and Cl^--$\delta^{18}O$ ratio 112

4.5 Discussion 114

4.5.1 Chances of seawater intrusion 114

4.5.2 Origin of the salinity 115

4.5.3 Extent of seawater mixing 117

4.6 Conclusion 120

Concluding Remarks 121

References 123

Abstract (Korea) 136

List of Figures

Pages

Chapter 2

Figure 2.1 Conceptual flow chart describing the process of combining a solute transport modeling with a multivariate regression analysis to develop a modeling tool for groundwater quality management. 13

Figure 2.2 Schematic illustration of the backward transport equation, which describes solute moving in the opposite direction to the groundwater flow. 15

Figure 2.3 Location of study site in Yupori, Chuncheon and groundwater pumping wells in the site. 21

Figure 2.4 Land use map of Yupori. Agricultural land use is in focus of this study, and types of land use are mapped into three agricultural types, which are orchard, barn, and vegetable field, and the other non-agricultural type, forest and residential area. 22

Figure 2.5 Model boundary and pumping well location for groundwater flow and solute transport simulation of Yupori site. The boundaries are set along the stream, river and hill ridges surrounding the site. 25

Figure 2.6 Four layers constituting the model domain. Hydrogeologic properties of each layer are given in Table 2. 26

Figure 2.7 Simulated hydraulic head distribution of the conceptual model of the Yupori site. 30

Figure 2.8 (a) Probabilistic capture zone of 10-year compted with the backward transport equation and (b) 100 m-radius circular zone drawn on the land use map. 40 m^3/day of pumping rate is applied for the both cases. 31

Figure 2.9 Calculated nitrate concentrations plotted against the observed nitrate concentrations at each pumping well for three different cases of Model 1, 2 and 3. 39

Chapter 3

Figure 3.1 Map of study site in Icheon and location of burial pits. 50

Figure 3.2 Monthly rainfalls of 2011 of Icheon (www.kma.go.kr) 52

Figure 3.3 Map of burial pits survey lines. Two burial pits are represented as yellow box. The upper pit is labeled A and the lower pit B. The eight electrical resistivity survey lines are in green solid line with its name (L1 – L8). 55

Figure 3.4 Model boundary and burial locations in the model domain. Triangular mesh of the top surface is also shown in the map. 57

Figure 3.5 Five layers constituting the model domain. Hydrogeologic properties of each layer are given in Table 3.1. 58

Figure 3.6 Relationships of saturation-relative permeability and pressure-saturation of each material for variably-saturated 60

Figure 3.7 The distribution of electrical resistivity measured along the survey line L1 and L8 on June 5th. 65

Figure 3.8 The distribution of electrical resistivity measured on June 5th along the survey line L3 and L4 which are located right down gradient of the lower burial pit, B. 67

Figure 3.9 The distribution of electrical resistivity measured on June 6th along the survey line L2 which are located at the down gradient of the upper burial pit, A. 68

Figure 3.10 Temporal distribution of the electrical resistivity at the vertical section of L3 on June 5th, August 23rd, and December 27th of 2011. 70

Figure 3.11 Initial hydraulic head distribution in the model domain from the simulation result. 72

Figure 3.12 Temporal distribution of ammonium on the vertical section of AA' at time 365, 1095, 1825, and 3650 day after the start of simulation. Ammonium is assumed to leak from the burial pits in the simulation model. 74

Figure 3.13 A vertical section of concentration distribution along a line equivalent to L2 at time of 120 day after the simulation, which roughly corresponds to the time of measurement in June. The yellow box in the figure shows the location of the upper burial pit. 77

Chapter 4

Figure 4.7 A schematic illustration of structure of an underground oil storage cavern. Types of water sample - injection water, monitoring well water, groundwater, and seepage water - are also shown (Lim et al., 2013) 84

Figure 4.2 Location of (a) Yeosu storage complex and the name of each cavern composing each storage base. Each cavern is represented as a rectangular. Open and solid circles in (b) and (c) are seawater intrusion barrier wells at the frontage of (b) the 1st and (c) the 2nd storage bases. Numbered circles are the wells where measurements were available and the numbers represent their name. 88

Figure 4.3 (a) Location of groundwater well near the caverns and the value of (b) EC, (c) Na^+, and (d) Cl^- at those wells plotted on the local map. 92

Figure 4.4 Box plot of Na^+ and Cl^- concentrations of (a) IW, MW, WT, and GW, (b) SW of the 1st base, (c) SW of the 2nd base and (d) SW of the 3rd base. Data for IW, MW, WT, GW and SW of the 1st and the 2nd bases are from 1999 to 2010, and for SW of the 3rd base are from 2008 to 2010. 97

Figure 4.5 EC profile by depth measured at the seawater intrusion barrier wells at (a) the 1st and (b) the 2nd storage bases. Numbers indicate the name of each well as shown in Figures. 4.2b and 4.2c. 100

Figure 4.6 Cl^-/Br^- ratios of different type of water samples from Yeosu storage complex. 103

Figure 4.7 PCA loadings for the first three components of the seepage water during the observation period between 1999 and 2010. 107

Figure 4.8 Plot of PC1 versus PC2 as the result of PCA of seepage water for 9 variables including pH, Ca^{2+}, K^+, Mg^{2+}, Na^+, Si, Cl^-, SO_4^{2-}, HCO_3^-. Those from the T101 and T102 caverns are bounded with solid line. 109

Figure 4.9 Plots of (a) δD versus $\delta^{18}O$ and (b) Cl^- concentration versus $\delta^{18}O$ for seepage and groundwater. The Global Meteoric Water Line (GMWL) is from Craig (1961) and Local Meteoric Water Line (LMWL) is from Lee and Lee (1999).

111

Figure 4.10 Bivariate plot of mixing ratios of seawater and the seepage water samples. The solid line in the plots represents the mixing line of seawater (Cl^- = 19,000 mg l^{-1}; Br^- = 65 mg l^{-1}) and local groundwater (Cl^- = 19 mg l^{-1}; Br^- = 1 mg l^{-1}).

113

List of Tables

Pages

Chapter 2

Table 2.1 Nitrate (NO_3-N) concentration at each pumping well of the site (in mg/L) 23

Table 2.2 Hydrogeologic properties used as input for model simulation 27

Table 2.3 Statistical review of the regression variables (STDEV: standard deviation) 33

Table 2.4 Description of three cases of model comparison 36

Table 2.5 Regression coefficient estimation result of three cases of Tobit regression 37

Chapter 3

Table 3.1 Hydrogeologic properties used as input for model simulation 59

Table 3.2 The IMED and Euclidean distance values between electrical resistivity measurement results of June, August and December and the simulation results at 120, 181, and 304 day of elapsed time after the start of simulation. 78

Chapter 4

Table 4.1 Na^+ and Cl^- concentrations measured at seawater intrusion barrier wells 101

Table 4.2 Cl^- concentration and Cl^-/Br^- ratios for different types of salinity 104

Table 4.3 Statistical data of the variables for PCA 106

Table 4.4 The maximum estimate of mixing ratio in seepage water (SW) at each cavern using the Cl^-–Br^- mixing ratio 119

Chapter 1 Introduction

Groundwater, while being the substantial source of fresh water, has been easily disregarded as it lies under the sight of our daily lives. However, the amount of groundwater that we use in our everyday life is beyond our awareness. The percentage of groundwater for potable supply is about 30% in Asia and reaches up to 70% in Europe (Morris et al., 2003), and 43% of the total irrigation water is from groundwater according to Siebert et al.(2010). Since the groundwater is closely related to human activities in many quarters, there can be various causes and processes which contaminate groundwater.

Meanwhile, groundwater system is an essential part of the hydrologic cycle and thus it sustains streams, lakes, wetlands as persistent sources and also as reservoirs to regulate the variability inherent in surface water supplies (Alley *at al*., 2002). The interaction of groundwater with other surface water systems is not just limited to the displacement of water itself but it influences on the solute transport. Thus groundwater, once contaminated, requires considerable amounts of time, effort, and expense to be cleaned and even for all that cost, it is not feasible to restore it to its state previous to contamination.

Thus, for sustainable use of groundwater, prevention of groundwater contamination in advance should be a top priority. For this reason, one needs to understand the hydrochemical characters of groundwater and pay attentions to potential contaminant sources by continuous of monitoring of groundwater quality. For the site where groundwater had already been contaminated, monitoring of groundwater is also an essential process to understand the causes of contamination, and then to avoid further contamination.

This study analyses sources of groundwater contamination from different causes in different environment. Studies in groundwater contamination have used various methods to have better understating of contaminant transport and fate in subsurface.

Modeling occupies one major niche of research methods in studying groundwater contamination. Various models have been developed by previous researchers and these include MODFLOW-2000 (Zheng et al., 2001), SUTRA (Voss, 1984), FEFLOW (Diersh, 2002), and HydroGeoSphere (Therrien et al., 2005). A mathematical modeling method requires hydraulic parameters and flow conditions necessary to solve differential equations for groundwater flow. In addition to this, analysis and prediction of contaminant transport requires information about transport conditions including the strength and extent of contaminant sources, which are not easily obtainable in many

field sites.

Another method commonly used in studying contaminated groundwater is using geochemical data. Stable isotopes of oxygen, carbon, nitrogen, hydrogen, and sulfur can provide useful information about their origins with which we can track the sources of our target contaminants (Kaown et al., 2009; Choi et al., 2007; Vandenschrick et al., 2002). Statistical methods are often used in conjunction with hydrochemical data. Principal component analysis (PCA), factor analysis (FA), and cluster analysis are methods used in general to reveal the internal structure of the given data with a large number of variables (Morell et al., 1996; Lee et al., 2007; Kaown et al., 2007; Lee et al., 2001)

Along with the above-mentioned mathematical modeling, and geochemical analysis, geophysical methods are widely used in detection of underground contamination. Electrical resistivity tomography, one of the most traditional geophysical methods, measures the electrical resistivity of subsurface that is strongly related to the effective porosity, the degree of saturation, and the pore water conductivity. Thus, the measure of electrical resistivity have been often used in hydrogeological characterization, such as monitoring moisture content and permeability of subsurface, and detection of solute distribution (Hubbard et al., 1997; van Overmeeren et al., 1997;

Daily et al, 2004; Ramirez et al., 1996).

Since groundwater contamination can be caused from multiple factors, analysis of contamination often needs to be approached with multiple methods which are appropriate for the site of investigation. This study suggests integration of different methods which are properly chosen according to the site specific characteristics when evaluating groundwater contamination.

In the first topic, modeling of solute transport is integrated into a regression method to analyze the effect of land use on groundwater quality and to predict contaminant concentration of groundwater in an agricultural region. A backward transport equation, which is a mathematical model based on the physical processes of solute transport, is used to delineate probabilistic capture zones. The probabilistic capture zone defines the area where contaminant discharge can have a direct influence, with relevant probabilities, on the quality of groundwater pumped from a well. Tobit regression analysis is used to find the relationship between independent regression variables and a dependent variable, which is contaminant concentration in this study. The capture zone and the regression are combined into a model, and its applicability for prediction of nitrate concentration is tested in a small agricultural basin in Chuncheon, Korea, which is occupied mainly by vegetation fields, orchards, and small barns.

The second topic is about leachate transport from livestock mortality burial during the decomposition of carcasses. Due to the specific character the site, there was only one well for monitoring and sampling groundwater and it was difficult to set up additional wells even for research purposes. In order to overcome the limitation of using monitoring wells, electrical resistivity tomography (ERT) is used as an alternative method to obtain data. The electrical resistivity measures were compared with the result of leachate transport model of the study site. The properties of the images from the two different methods were compared and analyzed for quantitative assessment of the simulation model to increase accuracy in prediction of leachate transport.

The last topic uses hydrogeochemical and isotopic indicators to assess the characteristics of salinized seepage into an underground oil storage cavern in a coastal area of Yeosu, Korea. The construction and operation of underground caverns can act as groundwater sinks near a coastal area. In an environment complicated with such artificial structures, seawater intrusion is not simple and thus needs to be evaluated by means of multiple analytical approaches. Cl^-/Br^- ratios, principal component analysis (PCA) of chemical data, and stable isotope data were used to determine the origin and the extent of salinization. These data were interpreted under the context of hydrogeological feature of the study area.

Chapter 2 Model-integrated regression analysis of groundwater contamination at an agricultural region

Abstract

Probabilistic capture zones are combined with a regression model and used as buffer zones around wells for Tobit regression analysis to predict contaminant concentration of groundwater in an agricultural region. A backward transport equation, which is a mathematical model based on the physical processes of solute transport, is used to delineate probabilistic capture zones. The probabilistic capture zone defines the area where contaminant discharge can have a direct influence, with pertinent probability, on the quality of groundwater pumped from a well. Tobit regression analysis is used to find the relationship between independent regression variables and a dependent variable, which is contaminant concentration in this study. The capture zone and the regression are combined into a model, and its applicability for prediction of nitrate concentration is tested in a small agricultural basin in Chuncheon, Korea, which is occupied mainly by vegetation fields, orchards, and small barns. Three cases of Model 1, Model 2, and Model 3 are compared in which buffer zones are circles, capture zones with probability over 0.1, and capture zones divided into sections with different probabilities,

respectively. The resulting regression model describes nitrate concentration in terms of selected independent variables. When the concentrations are calculated with the model, the best fit with the observed concentrations was in Model 3. This result supports the applicability of the method proposed in this study to prediction of contaminant concentration of groundwater.

2.1 Introduction

Contaminated groundwater requires considerable amounts of time, effort, and expense to be cleaned, and even for all that cost, it is almost impossible to restore it to its previous state. Thus, prevention of groundwater contamination should be a top priority for sustainable use of groundwater. Strategies for the management of groundwater quality can be established based on assessment of groundwater vulnerability and prediction of groundwater quality. The methods for vulnerability assessment and prediction of the groundwater quality can be classified into three categories: index method (Aller *et al*., 1987; Palmer and Lewis, 1998; Doerfliger *et al*., 1999; Kim and Hamm, 1999; Sener et al., 2009), mathematical modeling method (Frind *et al*., 2006; Lim *et al*., 2009), and statistical method (Eckhardt and Stackelberg, 1995; Tesoriero and Voss, 1997; Kroll and Stedinger, 1999; Nolan, 2001; Gardner and Vogel, 2005; Gurdak and Qi, 2006; Kaown *et al*., 2007; Stigter *et al*., 2008). Each method has its own advantages as well as limitations.

The advantage of index methods, which is basically a method of grading factors affecting groundwater quality, is that it is easy to practice. However, it can be subjective and biased when determining which factors to consider and how to grade those factors. This type of method has been modified using statistical methods for grading factors to

lessen its subjectivity (Panagopoulos *et al*., 2006; Antonakos and Lambrakis, 2007). However, the indices given as a result of analysis using an index method are still not suitable for quantitative management of groundwater quality.

One of the statistical methods used in general for prediction of groundwater quality is a Tobit regression method which is a multivariate regression analysis model, through which one can find a causal relationship between groundwater quality and other variables (Kroll and Stedinger, 1999; Gardner and Vogel, 2005; Kaown *et al*., 2007). Using this regression method, a circular zone enclosing a well is delineated to collect land use data near the well and its radius is decided considering the well's pumping rate and groundwater velocity (Barringer *et al*. 1990; Gardner and Vogel, 2005; Kaown *et al*., 2007;). The circular buffer zone, however, counts equal weight for the area inside the zone regardless of the hydraulic distance from the well. To improve this, a probabilistic capture zone of a well is delineated and used as a substitute of the circular zone in this study.

Mathematical modeling methods are based on the physical processes of groundwater flow and solute transport in an aquifer. Various models have been developed by previous researchers and these include MODFLOW-2000 (Zheng *et al*., 2001), SUTRA (Voss, 1984), FEFLOW (Diersh, 2002), and HydroGeoSphere (Therrien

et al., 2005). A mathematical modeling method requires hydraulic parameters and flow conditions necessary to solve differential equations for groundwater flow. In addition to this, analysis and prediction of contaminant transport requires information about transport conditions including the strength and extent of contaminant sources, which are not easily obtainable in regular field sites.

Recent studies in the field of groundwater quality management have implemented to combine methods in different framework to supplement limits of each method (Panagopoulos *et al*., 2006; Antonakos and Lambrakis, 2007; Moutsopoulos *et al*., 2008; Hesser *et al*., 2010).

The method proposed in this study is also a combination of two methods based on two different frameworks: a mathematical modeling and a statistical method. We employ the backward transport equation which describes solutes moving in the opposite of flow direction to come up with probabilistic capture zones. It has been introduced as an efficient method in delineating well protection zones in previous researches (Frind et al., 2006; Tosco and Sethi, 2010). The advantage of using this backward transport equation is that it enables us to delineate the affected area directly to groundwater extracted from a pumping well, while it does not require identified source conditions. In addition, the capture zone also can be represented in a probabilistic way that is

appropriate for quantitative estimation of groundwater contamination. All the regression variables are measured within this capture zone and then a model combining a mathematical model with a regression model is established.

The objective of this study is to develop a statistically parameterized model for prediction of groundwater contamination with the combined use of a mathematical modeling and a statistical method to take advantage of the strengths of each. A method for prediction of groundwater contamination with a statistically parameterized model associated with land use patterns can provide information on management priorities for land use for effective groundwater quality protection. In addition to that, the method is useful in identifying the wells affected by a local point contaminant source that causes deviations from regional contaminant concentration levels.

2.2 Methods

The method proposed in this study is based on two different methods: a solute transport model and a multivariate regression analysis. The process combining the two different methods is described in Figure 2.1. The probabilistic capture zones are delineated with the backward transport equations and then all the regression variables including land use area are measured within the capture zones. Finally, regression

analysis with the Tobit method is performed to obtain the prediction model. Topographic data measured at the locations of pumping wells and the measure of land use area within the probabilistic capture zone of those wells are used as independent variables for the regression analysis. Detailed descriptions of each method are given below.

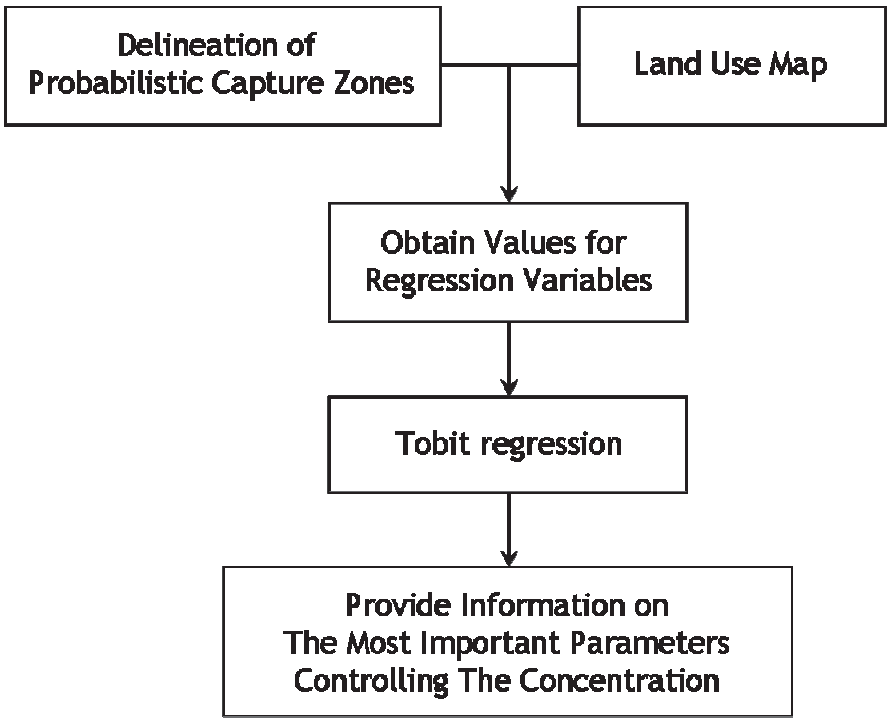

Figure 2.1 Conceptual flow chart describing the process of combining a solute transport modeling with a multivariate regression analysis to develop a modeling tool for groundwater quality management.

2.2.1 Delineating probabilistic capture zone

Solute movement in groundwater can be described using the advection-dispersion equation given as follows:

$$\theta \frac{\partial C}{\partial t} = -\frac{\partial}{\partial x_i}(\theta v_i C) + \frac{\partial}{\partial x_i}\left(\theta D_{ij} \frac{\partial C}{\partial x_j}\right) + q_{\mathrm{I}} C_{\mathrm{I}} - q_{\mathrm{O}} C \qquad [2\text{-}1]$$

where C [M L^{-3}] is solute concentration, t [T] is time, θ [-] is the porosity of an aquifer material, v_i [L T^{-1}] is groundwater velocity in the x_i direction, D_{ij} [L^2 T^{-1}] is the dispersion coefficient, q_{I} [T^{-1}] is the inflow rate per unit volume, q_{O} [T^{-1}] is the outflow rate per unit volume, and C_{I} [M L^{-3}] is solute concentration of the inflow.

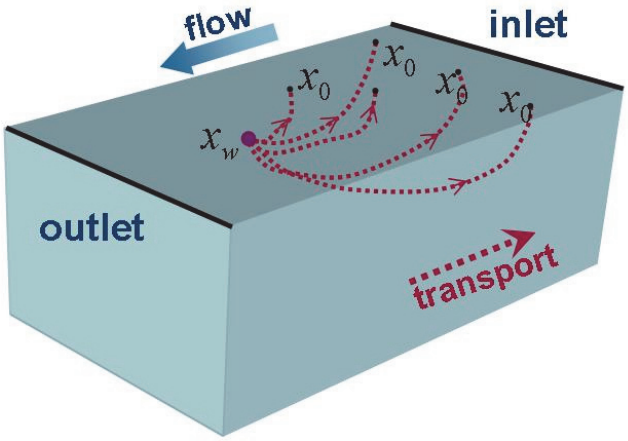

Figure 2.2 Schematic illustration of the backward transport equation, which describes solute moving in the opposite direction to the groundwater flow.

A backward transport equation, which describes solute moving in the opposite direction to the groundwater flow (Figure 2.2) is derived from the Eq. [2-1] above. The backward equation, which is an adjoint equation of the advection-dispersion equation, Eq. [2-1], is given as follows (Neupauer and Wilson, 1999, 2001):

$$\theta \frac{\partial \psi^*}{\partial \tau} = \frac{\partial}{\partial x_i}\left(\theta v_i \psi^*\right) + \frac{\partial}{\partial x_i}\left(\theta D_{ij} \frac{\partial \psi^*}{\partial x_j}\right) - q_I \psi^* \qquad [2\text{-}2]$$

where τ is time in backward, and ψ^* [L^{-3}] is an adjoint state of the original variable C. The adjoint state ψ^* is defined as the ratio of the solute concentration at a pumping well to the initial solute mass, given as follows (Neupauer and Wilson, 1999, 2001):

$$\psi^*(x_0, \tau; x_w) = \frac{dC(x_w, t)}{dM_0(x_0)} \qquad [2\text{-}3]$$

where ψ^* (x_0, τ; x_w) is the adjoint state of solute concentration C at a position of a pumping well x_w located down-gradient of the source injection point x_0, and M_0 is the initial solute mass injected at x_0. Using the backward equation of Eq. [2-2] with the adjoint state defined as in Eq. [2-3], one can estimate quantitatively the influence of a potential contaminant source on the quality of groundwater extracted from a pumping well with neither information about the location of contaminant sources nor repeated computations.

When the solute concentration C is defined as flux concentration C^f which is a

measure of solute mass passing through a fixed location per unit water flux at a given time, normalizing C^f with the total solute mass released from the source represents a probability density function of time required for solute particles to travel from its release point to a location of interest. This is written as follows (Neupauer and Wilson, 1999, 2001; Cornaton, 2003):

$$f_{\mathrm{t}}(t;x)=\frac{C^{\mathrm{f}}(x,t)}{\int_0^{\infty}C^{\mathrm{f}}(x,t)\mathrm{d}t}=\frac{C^{\mathrm{f}}(x,t)}{M_0/A(x)q(x,t)} \qquad [2\text{-}4]$$

where $f_{\mathrm{t}}(t, x)$ is the travel time probability density function at location x, the integral of $C^f(x, t)$ is a measure of the total solute mass per unit water flux at location x, A is the area perpendicular to flow, across which the flux concentration is defined, and q is the groundwater discharge. The travel time probability density function can be rearranged for solute traveling from x_0 to x_{w} as follows (Neupauer and Wilson, 1999, 2001; Cornaton, 2003):

$$f_{\mathrm{t}}(t;x_{\mathrm{w}},x_0)=\theta(x_{\mathrm{w}})\left|q(x_{\mathrm{w}},t)\right|A(x_{\mathrm{w}})\frac{\mathrm{d}C^{\mathrm{f}}(x_{\mathrm{w}},t;x_0)}{\mathrm{d}M_0}=\theta(x_{\mathrm{w}})\left|q(x_{\mathrm{w}},t)\right|A(x_{\mathrm{w}})\psi_{\tau}^{*}(x_0,\tau;x_{\mathrm{w}}) \qquad [2\text{-}5]$$

where ψ_{τ}^{*} is the adjoint state of C^f.

The integral of Eq. [2-5] represents the probabilistic capture zone which describes the probability of solutes to be captured at x_{w} within a given time t. This can be written as follows (Cornaton, 2003):

$$F_{\mathrm{t}}(t;x_{\mathrm{w}},x_0)=\theta(x_{\mathrm{w}})\left|q(x_{\mathrm{w}},t)\right|A(x_{\mathrm{w}})\int_0^t\psi_\tau^*(x_0,\tau;x_{\mathrm{w}})\mathrm{d}t \qquad [2\text{-}6]$$

where $F_{\mathrm{t}}(t; x_{\mathrm{w}}, x_0)$ is the probability of a solute discharged at a source injection point x_0 to be detected at a pumping well at x_{w} within time t. The probabilistic capture zone delineated using Eq. [2-6] is based on the advection-dispersion equation describing physical processes of solute transport in an aquifer and is characterized by its probabilistic representation of source impact on groundwater at a pumping well location which varies even within one capture zone. Therefore, data collected within a probabilistic capture zone are expected to show a stronger relationship with the contaminant concentration of groundwater than those within a circular zone. HydroGeoSphere (Therrien *et al*., 2005), a three-dimensional flow and transport model, is used for calculating the backward transport equation and delineating probabilistic capture zones of pumping wells.

2.2.2 Tobit regression

The Tobit method is a multivariate regression analysis method for censored data estimating regression coefficients for independent variables using maximum likelihood estimation to find the relationship between a dependent variable and independent variables. When the data being used as dependent variable are censored, i.e. existing

only within a certain range, using Tobit regression can prevent the analysis result from being biased or inconsistent (Yen *et al*., 1996; Liu *et al*., 1997). In this study, contaminant concentrations observed at pumping wells are assigned as the dependent variable and Tobit regression method is applied, since we are interested only in concentration values above a background concentration. The Tobit regression model can be written as follows:

$$q_i^* = \ln(C_i)^* = \alpha + \overline{\beta} \ln(\overline{p}_i) + \varepsilon_i \qquad \text{[2-7a]}$$

$$q_i = \begin{cases} q_i^* & \text{if } C_i > c \\ \ln c & \text{otherwise} \end{cases} \qquad \text{[2-7b]}$$

where q_i^* is the latent dependent variable, q_i is the observed dependent variable, C_i [M L^{-3}] is the observed contaminant concentration, α is a constant, $\overline{\beta}$ is a vector of regression coefficient estimates, $\ln(\overline{p}_i)$ is a vector of independent variables, and ε_i is a residual error term which is assumed to be normally distributed with zero mean and variance σ^2. The observed dependent variable q_i can be represented as the latent dependent variable q_i^* when the contaminant concentration C_i is above a given threshold value c, or as ln$c$ otherwise (Tobin, 1958; Kroll and Stedinger, 1999; Gardner and Vogel, 2005).

In the Tobit model, the significance of each independent variable in relation to the

dependent variable can be evaluated by the Wald chi-square statistic which shows the ratio of the estimates of a regression coefficient to its standard error (Wald, 1945). The larger the value of Wald chi-square, the more significant the effect that an independent variable has on the dependent variable. Estimates of regression coefficients are calculated using statistical analysis software SAS (SAS Institute, 2003).

2.2.3 Model-integrated regression analysis

2.2.3.1 Site Description

The developed model is applied to Yupori, a small agricultural basin located in Chuncheon, Korea (Figure 2.3) to examine the applicability and efficiency of the method. The study site is mostly occupied by orchards, vegetable fields and barns (Figure 2.4) and surrounded by hills on its western and eastern boundaries, and by streams on its southern and northern boundaries. The groundwater quality in Yupori had been monitored for several years through groundwater samples from 42 pumping wells in the area. Nitrate was observed to be one of the most threatening contaminants at the site probably because of frequent use of chemical fertilizers and manures for agricultural purposes. Nitrate concentrations analyzed from groundwater samples are summarized in Table 2.1.

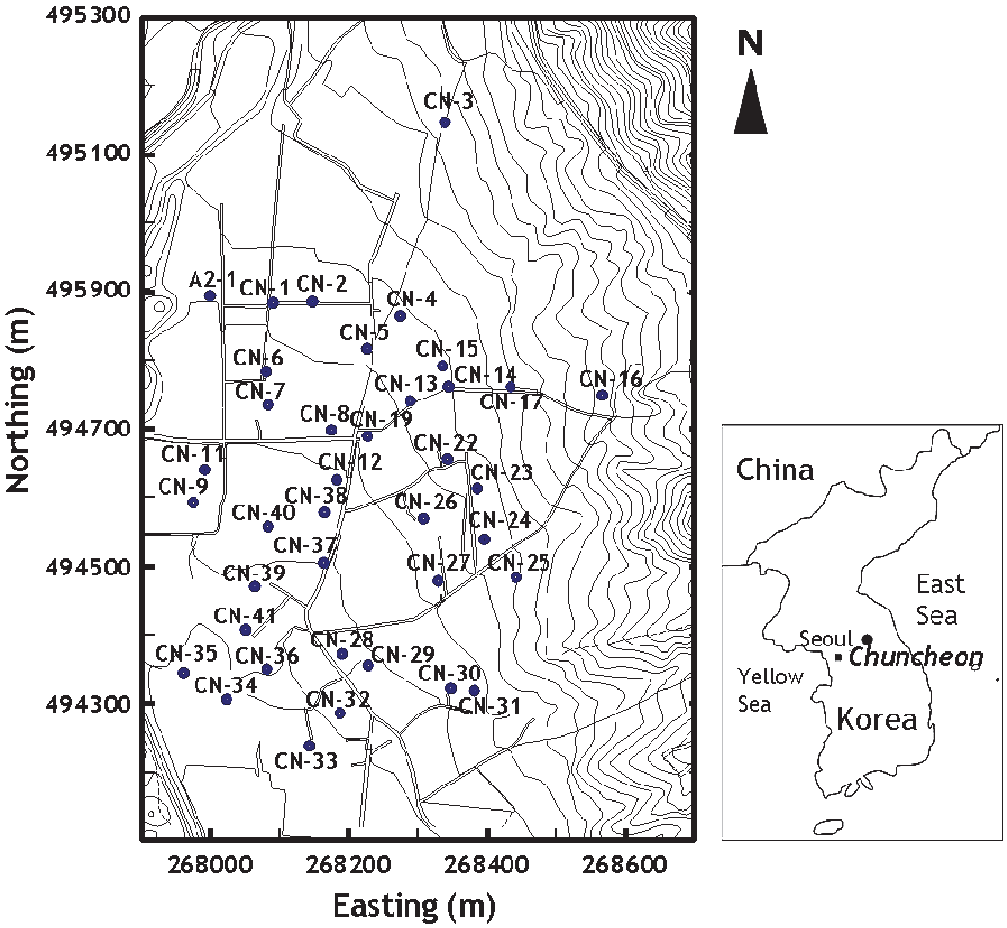

Figure 2.3 Location of study site in Yupori, Chuncheon and groundwater pumping wells in the site.

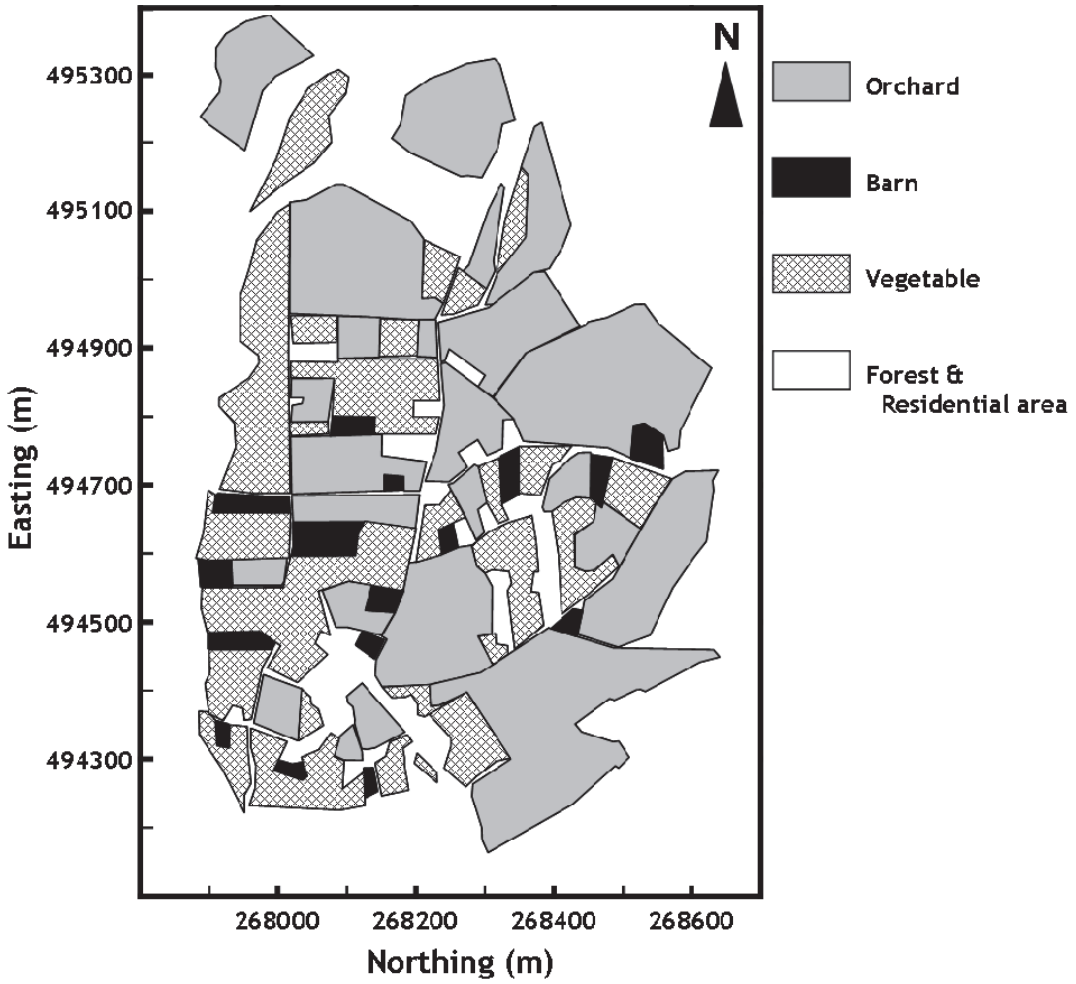

Figure 2.4 Land use map of Yupori. Agricultural land use is in focus of this study, and types of land use are mapped into three agricultural types, which are orchard, barn, and vegetable field, and the other non-agricultural type, forest and residential area.

Table 2.1 Nitrate (NO_3-N) concentration at each pumping well of the site (in mg/L)

Pumping Well	Sampled Date					
	Feb. 2003	Jun. 2003	Aug. 2003	Aug. 2003	Dec. 2003	Aug. 2004
A2-1	19.3	17	9.8	16	21.1	15.0
CN-01	3.2	6.1	11	5.3	-	6.0
CN-02	0.2	0.3	0.2	0.2	0.4	0.2
CN-03	0.6	1.4	1.2	1.6	1.7	1.0
CN-04	0.7	1.1	1.1	0.2	0.4	0.3
CN-05	3.9	5	4	4.9	5.2	4.4
CN-06	16.0	18.7	20	13.5	18	21.6
CN-07	17.5	16.9	20.5	16.8	23.4	21.4
CN-08	4.9	6.4	6.1	3.8	4.3	6.8
CN-09	20.4	17	16.2	16.3	21.6	16.6
CN-10	-	-	-	-	-	
CN-11	20.1	13.5	13.4	17.1	23.4	18.3
CN-12	4.1	4.7	3	3.8	4.8	4.8
CN-13	3.8	3.7	3.2	3.1	3.8	6.0
CN-14	0.1	1.2	1.1	1	1.4	1.0
CN-15	0.3	0.7	0.6	0.5	0.7	0.6
CN-16	0.5	1	0.9	0.9	1.2	1.0
CN-17	-	1.6	1.5	1.5	2.3	-
CN-18	-	-	-	-	-	-
CN-19	4.2	5.4	5	3.6	6.4	6.0
CN-20	1.7	2.9	2.8	1.1	1.5	-
CN-21	2.2	2.7	2.8	1.2	1.9	-
CN-22	0.8	1.6	1.3	1.4	2.2	2.1
CN-23	0.5	0.6	0.5	0.4	0.7	0.6
CN-24	1.9	2.4	2.2	1.9	2.7	2.6
CN-25	0.2	1.2	0.4	0.8	1.1	0.7
CN-26	0.8	1.6	3	0.9	1.2	1.1
CN-27	1.0	1.5	4.7	1.4	1.8	1.3
CN-28	4.3	13.6	18.2	3.9	4.7	8.2
CN-29	-	14	14.8	3.4	4.7	7.5
CN-30	0.5	0.9	2.4	0.4	0.6	0.8
CN-31	1.1	1.9	3.2	1.6	2.2	1.9
CN-32	3.4	3.7	16	2.3	3.5	4.2
CN-33	4.0	6.1	5.7	5	6.3	5.5
CN-34	5.9	15.1	15.6	16.5	24	25.4
CN-35	15.2	20.6	20.9	11	30.1	19.5
CN-36	7.0	7.9	8.6	5.9	8.8	8.7
CN-37	-	7.4	6.9	3.4	6	4.8
CN-38	5.6	6.5	5.5	4.4	6.6	5.5
CN-39	-	10	12.7	9.6	-	12.2
CN-40	4.4	6.9	7.9	8.7	12.8	9.7
CN-41	9.4	13.4	19	7.4	8.8	12.3

The geological structure of the site consists of weathered Chuncheon granite overlain by unconsolidated Quaternary alluvium of 10 to 20 m thickness, which is characterized by alternation of silty sand and coarse grained sediments (Yu *et al*., 1994).

2.2.3.2 Application

A conceptual model is built to simulate the groundwater flow and solute transport of the site. Model boundaries are set along the stream, river and hill ridges surrounding the site as illustrated in Figure 2.5 in which the area shown in Figures 2.3 and 2.4 is indicated with a double lined box. The domain is divided into four layers (Figure 2.6) and hydrogeologic properties for each layer are given as in Table 2.2 referring geological structure and the hydraulic test results of Kaown *et al*. (2007).

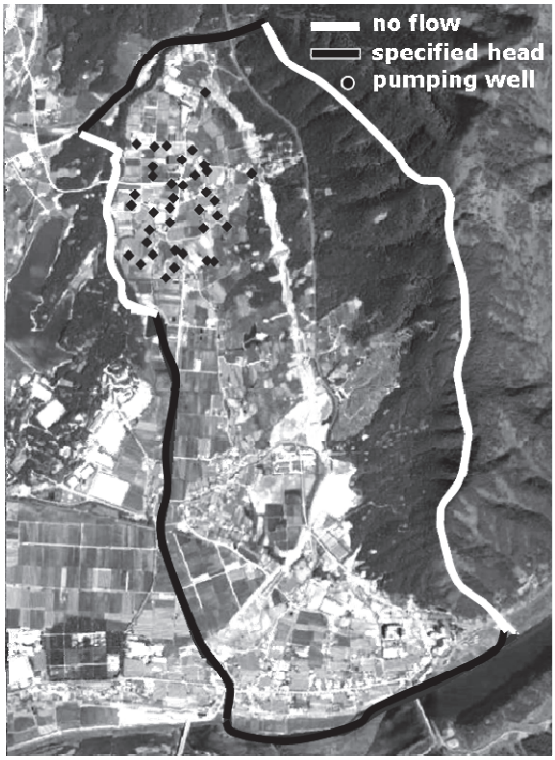

Figure 2.5 Model boundary and pumping well location for groundwater flow and solute transport simulation of Yupori site. The boundaries are set along the stream, river and hill ridges surrounding the site.

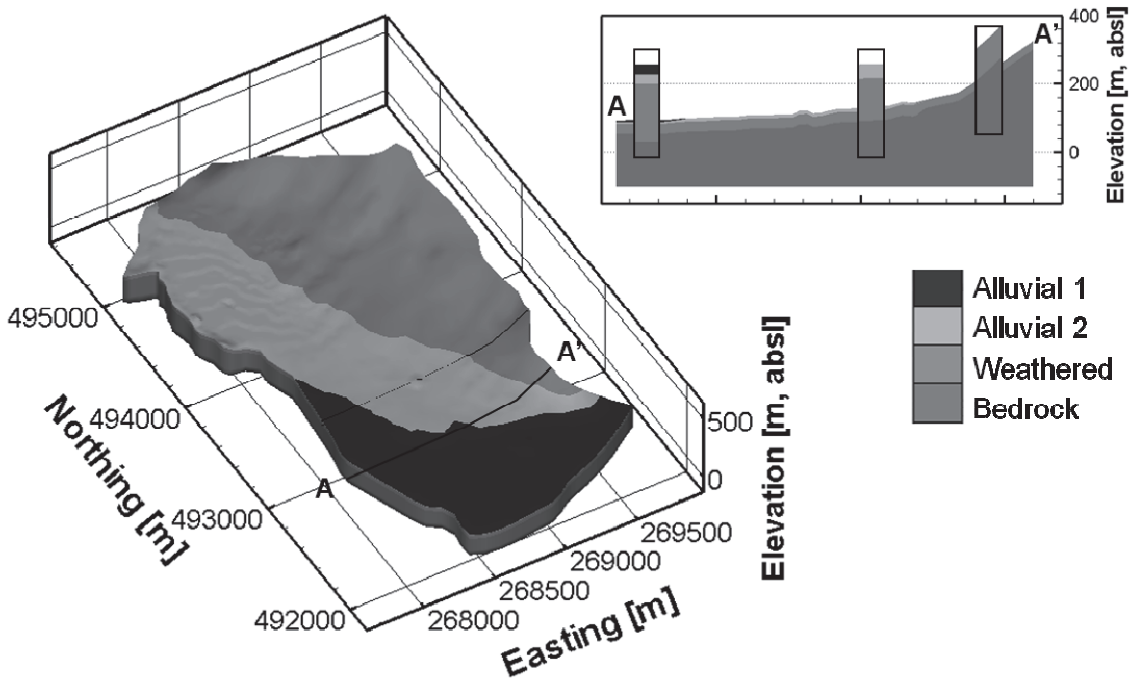

Figure 2.6 Four layers constituting the model domain. Hydrogeologic properties of each layer are given in Table 2.

Table 2.2 Hydrogeologic properties used as input for model simulation

Property	Alluvial 1	Alluvial 2	Weathered	Bedrock
Hydraulic Conductivity [cm sec^{-1}]				
Kx	1.04×10^{-3}	9.26×10^{-3}	9.95×10^{-5}	1.16×10^{-9}
Ky	1.04×10^{-3}	9.26×10^{-3}	9.95×10^{-5}	1.16×10^{-9}
Kz	1.04×10^{-4}	9.26×10^{-4}	9.95×10^{-6}	1.16×10^{-9}
Porosity [-]	0.3	0.3	0.35	0.01
Dispersivity [m]				
α_L	8	8	8	8
α_T	0.8	0.8	0.8	0.8
Tortuosity [-]	0.1	0.1	0.1	0.1

Figure 2.7 shows the simulated hydraulic head distribution of the study site and it shows that groundwater is flowing from hill slope in the eastern part of the area to the streams on the southern and northern boundaries. In particular, in the region where the pumping wells are located, groundwater is flowing mainly in the south-western direction.

The pumping rate for each of the 42 wells was about 40 $m^3 day^{-1}$ and, given this condition, the probabilistic capture zone of a 10-year period is delineated as illustrated in Figure 2.8(a). Contour lines on the figure represent probability of 0.1, 0.3, 0.5, 0.7 and 0.9 from the outermost to the innermost line respectively. It is noticeable that the capture zones are elongated in the direction opposite to the groundwater flow, which evokes the influence of groundwater flow in delineating the capture zones. The size of the probabilistic capture zone varies for different given times and a 10-year capture zone is chosen since recharge from ground surface to groundwater table at the site is known to take about 10 years (Kaown *et al*., 2009). These capture zones are to be used as buffer zones for Tobit regression to find out relevant factors affecting nitrate concentration of groundwater and to build a combined model to estimate nitrate concentration. As a comparison in validating the efficiency of the method, a circular zone of 100m-radius is drawn around each well for Tobit regression (Figure 2.8(b)). The

radius of the circular area is determined with regards to the time of recharge and hydraulic conductivity of the study area (Kaown *et al*., 20007).

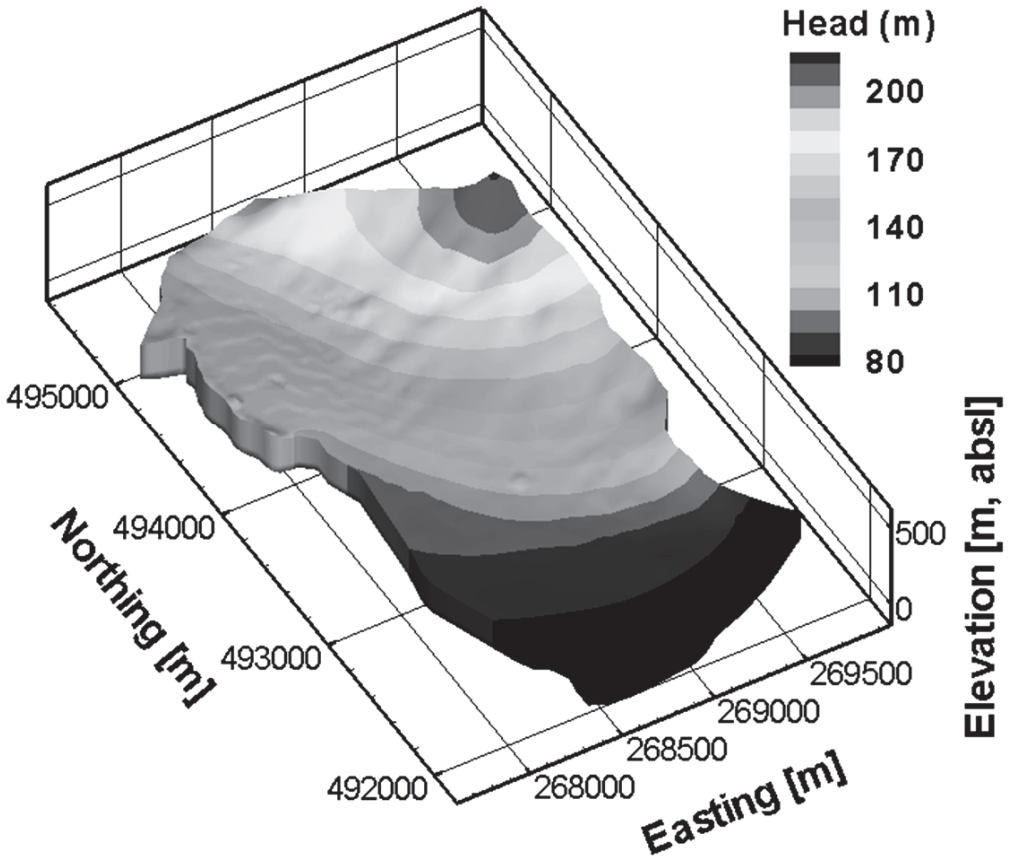

Figure 2.7 Simulated hydraulic head distribution of the conceptual model of the Yupori site.

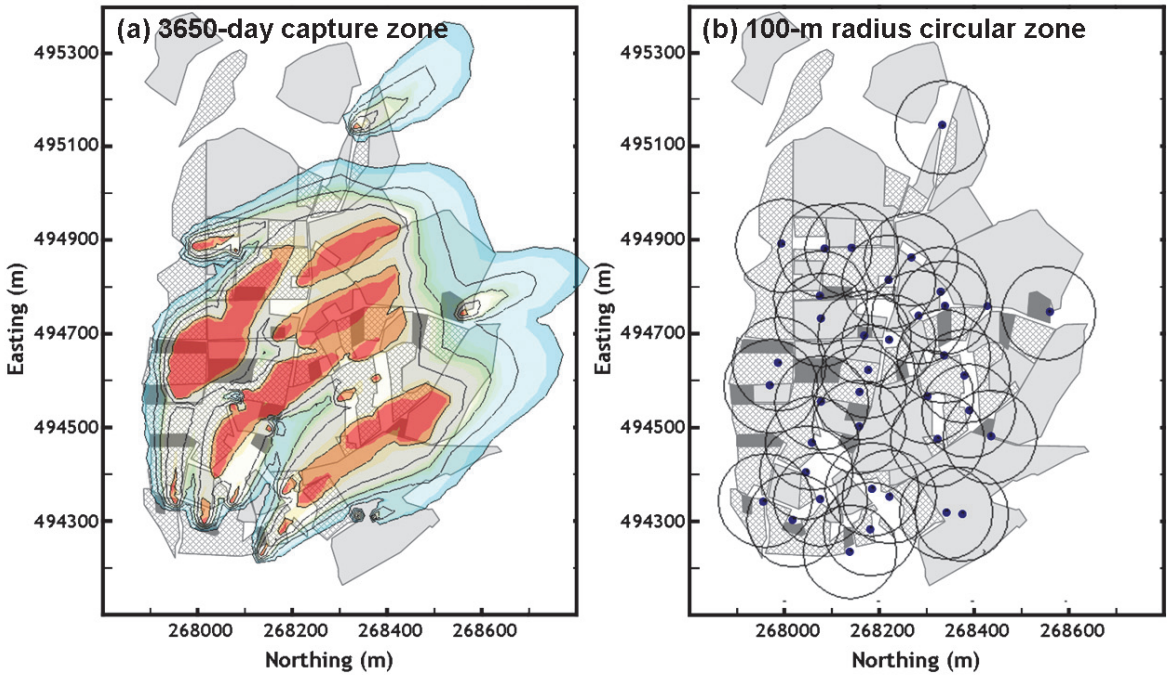

Figure 2.8 (a) Probabilistic capture zone of 10-year compted with the backward transport equation and (b) 100 m-radius circular zone drawn on the land use map. 40 m^3/day of pumping rate is applied for the both cases.

For Tobit regression, the observed nitrate concentrations are assigned as dependent variables and elevation, slope, well-depth, and the area of each type of land use—vegetable field, barn, or orchard— are independent variables. Topographic data and land use area are chosen as independent variables since the former data are suspected to be relevant to the physical processes of solute transport and the latter is closely related to the amount of fertilizers and manures which are the possible main source for nitrates in the study site. The size of the land use area is the factor differentiating the two methods using circles or capture zones as buffer zones as seen in Figure 2.8. Statistical results of each regression variable are given in Table 2.3. The censoring threshold value, *c* in Eq. [2-7b] is given as 2.6 mg L^{-1} NO_3-N, for it is estimated to be the background concentration in groundwater and surface water of the study site (Kaown *et al*., 2007) and our interest is focused on nitrate concentration exceeding the background concentration.

Table 2.3 Statistical review of the regression variables (STDEV: standard deviation)

Variable	Mean	Minimum	Maximum	Median	STDEV
Topographic data of well location					
Slope (°)	3.44	0.0	13.50	2.96	2.03
Elevation (m)	130.63	116.60	162.90	130.0	9.74
Well depth (m)	36.32	6.0	100.00	30.0	20.32
Land use data (m^2)					
VE†	9759.85	0.0	26736.54	9315.67	7583.61
BRN	1914.27	0.0	6875.77	1302.50	2022.27
ORD	19264.09	1438.33	32733.81	20095.23	8085.45
Land use data with probability (m^2)					
VE1	5613.94	0.0	16162.53	4586.53	4756.37
VE4	2966.24	0.0	12605.13	1972.69	3175.70
VE7	1179.67	0.0	5420.53	530.27	1501.48
BRN1	1323.28	0.0	5122.79	683.57	1545.89
BRN4	427.10	0.0	2472.54	94.88	623.35
BRN7	163.88	0.0	1552.77	0.00	412.15
ORD1	13550.48	960.97	23763.58	13985.45	5773.22
ORD4	4419.54	0.0	10910.79	4419.71	2867.60
ORD7	1294.07	0.0	5863.65	748.04	1568.13

† VE= area of vegetable field; BRN= area of barn; ORD=area of orchard; *prefix*1=area of *prefix* with probability from 0.1 to 0.4; *prefix* 4=area of *prefix* with probability from 0.4 and 0.7; *prefix* 7=area of *prefix* with probability over 0.7.

To evaluate the efficiency of the method in prediction of contaminant concentration, three different cases are tested and compared. Model 1 follows the approach which has been used by previous researchers (Gardner and Vogel, 2005; Kaown *et al*., 2007). A circular zone of 100 m-radius around each pumping well is used as a buffer zone for Tobit regression and each type of land use area is measured within those circles and assigned as independent variable. Model 2 and Model 3 use 10-year probabilistic capture zones instead of circular zones for Tobit regression. In Model 2, land use area is measured within a capture zone of probability over 0.1.Solutes released within this zone are expected to be captured at the pumping well within 10 years with a probability of more than 0.1. In Model 3, more attention is given to the probability values and the capture zone is divided into three different sections of probability from 0.1 to 0.4, probability from 0.4 to 0.7, and probability over 0.7. Land use area is measured within each section of the capture zones with different probability range and these are used as independent variables separately.

The variables to be left in the final regression model because of their significance in their relationship with the observed nitrate concentration are chosen based on their p-value. It is the probability that null hypothesis explains the relationship of observed nitrate concentration and the other variables. The variables are considered to have

significance in relationship with nitrate concentration when the p-value is smaller than, in general, 0.05 (Dallal, 2007). Among the independent variables, the one with the largest p-value is eliminated and the regression analysis is repeated with the remaining variables until there are three major variables left with acceptable p-values.

2.3 Results & Discussion

Table 2.4 summarizes the results of coefficient estimates from the regression model using a data set observed in December 2003. Different variables are chosen to have a significant effect on the observed nitrate concentration for different cases of Models 1, 2 and 3. From the p-value, it can be said that the regression model of Model 3, in which capture zones are divided into sections with different probability, is statistically most significant among the three.

Regression analysis is repeated for the other data sets in Table 2.1 and the three most significant variables are listed in Table 2.5 in the order of their explanatory power in the model.

Table 2.4 Description of three cases of model comparison

Regression Model with Circular Zones	
Case 1	Land use area measured within a circular zone of each pumping well.
Hybrid Regression Model with Probabilistic Capture Zones	
Case 2	Land use area measured within a capture zone of probability 0.1 and more.
Case 3	Divided probabilistic capture zone. Land use area measured within capture zone of probability from 0.1 to 0.4, from 0.4 to 0.7, and above 0.7.

Table 2.5 Regression coefficient estimation result of three cases of Tobit regression

Variable	Estimate	STD Error	Chi-Square	Pr>ChiSq
Case 1				
VE	2.1914	0.7338	8.92	0.0028
BRN	5.0494	1.9597	6.64	0.01
Elevation	-0.0278	0.0104	7.19	0.0073
Case 2				
VE	35.7475	16.241	4.84	0.0277
BRN	204.4763	64.0934	10.18	0.0014
ORD	26.0489	12.1544	4.59	0.0321
Case 3				
VE1	73.5853	16.6379	19.56	<.0001
VE7	308.3117	51.1256	36.37	<.0001
ORD7	187.8803	49.3382	14.5	0.0001

Nitrate concentration at each pumping well is calculated using the resulting regression models and these are compared with the observations. When comparing the calculated with the observed, only the data observed to be above the censoring threshold, the background concentration of 2.6 mg L^{-1} NO_3-N, are included because the regression analysis is aimed to find a relationship between independent variables and nitrate concentration exceeding the background concentration. The correlation coefficients and errors between calculated and observed results are also summarized in Table 2.5.

The regression variables chosen to have significance in Model 1, which uses circular zones for Tobit regression, are different for each data set. However, the variables chosen in the model for Model 2 and Model 3, which use the probabilistic capture zones show consistency with identical variables for all data sets. In addition to that, estimation of nitrate concentration is also better when probabilistic capture zones are used, showing less error and more correlation when compared with the observed concentration. In particular, when the probability values are concerned as in Model 3, the calculated concentrations show better fit with the observed than in Model 2. Nitrate concentrations calculated are plotted against the observed ones and this is illustrated in Figure 2.9.

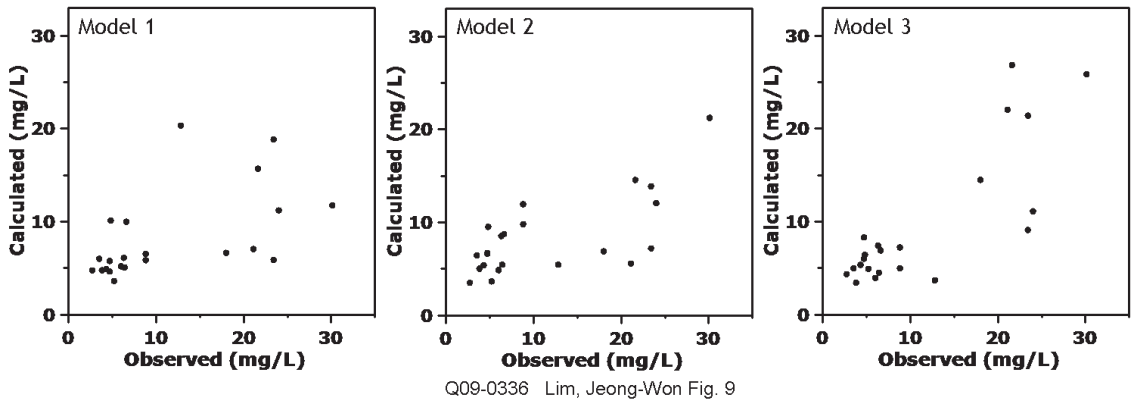

Figure 2.9 Calculated nitrate concentrations plotted against the observed nitrate concentrations at each pumping well for three different cases of Model 1, 2 and 3.

These results imply that combining probabilistic capture zones into regression analysis strengthens the regression model in reflecting processes of groundwater flow and solute transport more efficiently than using circular zones and thus increase its potential as an estimation model. What deserves some attention is that Model 3 which divides capture zones into sections with different probability gives the most significant regression model composed of independent variables with sufficiently small p-values and the calculated concentration using this model shows the best fit with the observed among the three models compared.

Areas of land uses appeared to be significant to the nitrate concentration in Model 2 and 3. The study site is an agricultural region and land uses of the site were mainly agricultural land, and fertilizers and manures which could be a major source of nitrate in groundwater are applied onto the agricultural land. The areas of land use variables are supposed to be surrogates for the amounts of fertilizers and manures applied on each type of agricultural land, and thus appeared to have significance to the nitrate concentrations in the regression analysis.

An area of barns, which is chosen as the most significant variable in Model 2, is withdrawn in Model 3. When probability values are concerned, vegetable fields and orchards in the zone of high probability seem to have more influence than barn. Barns

could be a strong source of nitrate in groundwater, but due to their small area, their influence becomes less significant when the probability is calculated over the full area of the capture zone. In Model 3, zones of vegetable fields and orchards, specifically with probabilities over 0.7, appeared to have large influence on the nitrate concentration of groundwater. Vegetable fields within the zone of probability from 0.1 to 0.4 are supposed to be chosen due to their rather spacious area, because the amount of fertilizer applied increases proportionally to the area of application.

Table 2.5 shows that regression model results can vary according to the way that data are collected even within a same field site. It demonstrates that establishing a reasonable regression model is a crucial matter to understand the factors affecting groundwater contaminant concentration. The proposed method takes advantage of probabilistic capture zones based on physical processes of solute transport, combines it with regression analysis, then finds significant variables affecting groundwater quality and in estimating contaminant concentrations at pumping wells.

2.4 Conclusion

In this study, a numerical modeling method is combined with a multivariate regression model to develop a parameterized prediction model for contaminant

concentration of groundwater in an agricultural region. A numerical model including backward transport is used to delineate probabilistic capture zones of pumping wells as well as to take into consideration the physical processes of groundwater flow and solute transport in an aquifer. As for the multivariate regression model, the Tobit regression method is used to analyze the relationship between the observed contaminant concentrations and other independent variables: topographic features and land uses. When measuring land use area, a probabilistic capture zone for each pumping well is used instead of the classical circular zone around a pumping well, so that we take advantage of both the numerical modeling and the regression analysis methods.

The regression model with probabilistic capture zones is applied to an agricultural area in Chuncheon, Korea and its results are compared with that of the regression model with circular zones. The models with probabilistic capture zones are consistent in choosing significant variables affecting nitrate concentration while the other is not. It is also noticeable that the model describing relationship of nitrate concentration with dependent variables is most robust statistically in Model 3, when capture zones are divided into sections with different probability.

The analysis results suggest land use as a significant factor affecting nitrate concentration in groundwater. Since the main source of nitrate contamination in the

study area is suspected to be fertilizers and manures from agricultural activities, this result seems reasonable. This result, that anthropogenic activities, specifically types of land use, are closely related to the nitrate concentration, is consistent with the findings of previous research (McLay *et al*., 2001; Lambrakis *et al*., 2004, Panagopoulos *et al*., 2006)

The estimated concentrations using Model 3 represent reasonable conformity with the observed concentrations. This method can be applied to groundwater management when contaminant concentrations violate a given standard of groundwater quality. The model can be used in estimating concentrations when significant independent variables are regulated and in validating whether the estimations are satisfying a given standard.

In all, the model combining the Tobit regression model with the probabilistic capture zones performs better in analyzing the relations between land use and groundwater quality and also in estimating contaminant concentration than the regression model with circular zones. The method is appropriate for application to groundwater quality management, with its relative simplicity in estimating groundwater quality compared to numerical modeling, as well as with its strength in finding factors controlling groundwater quality.

Chapter 3 Analysis of leachate transport at a livestock burial site using a model validated with geophysical data

Abstract

Understanding spatio-temporal variation of solute distribution in subsurface is a challenging assignment, in particular, when there is only limited number of observation wells in the area of interest. In this study, in order to overcome the spatial limitation of monitoring observation wells, electrical resistivity survey of subsurface is measured over a period of time and solute distribution is inferred from those resistivity results. The measure of the electrical resistivity has been performed several times during 2011 to observe leachate transport from a livestock mortalities burial in a rural area of Korea. A process based model describing flow and transport in a variably saturated zone has been built to represent the burial site of this study. The electrical resistivity measurement results show abnormally low resistivity zones which are supposed as leachate leakage from the burial. The results of modeling and electrical resistivity are used in combination to obtain quantitative analysis of leachate distribution using an image similarity metric. The image Euclidean distance between the simulation result and resistivity measure is calculated to represent the similarity of the two result and thus

to validate the simulation model which can be used in analyzing the influence of leachate in the area.

3.1 Introduction

When investigating a region for groundwater contamination, obtaining hydrogeologic and hydrogeochemical data is a fundamental step. A model representing the site of investigation is built employing those data and then the model is applied in analyzing the flow and transport system and then predicting the future behavior of the system.

The data are often collected through monitoring groundwater wells and analyzing samples from those wells. Thus a good geographical distribution of wells is critical in setting up a credible model of a region.

However, in many cases, it is not easy to obtain satisfying data neither in its quantity nor in quality. Existing wells may not be properly distributed to meet the purpose of investigation or there may not be enough number of wells available for monitoring and sampling. In addition, the access to many of contaminated sites is often limited, which makes it difficult to set up additional wells even for research purposes.

The site of this study was a livestock burial which is built during the nationwide outbreak of Foot-and-mouth disease, and there was only one well which we can use for monitoring and sampling groundwater.

In this study, in order to overcome the limitation of using monitoring wells,

electrical resistivity survey is used as an alternative method of obtaining data.

The electrical resistivity of subsurface is strongly related to the effective porosity, the degree of saturation, and the pore water conductivity. Thus, the measure of electrical resistivity have been widely used in hydrogeological characterization, such as monitoring moisture content and permeability in the subsurface (Hubbard et al., 1997; van Overmeeren et al., 1997; Daily et al., 1992). It also has been used in determining hydraulic conductivity to be employed for numerical groundwater modeling (Koukadaki et al. 2007).

In addition to parameterising aquifer properties, the electrical resistivity data have been used in detecting solute distribution and calibrating hydrological model for estimating solute distribution. Electrical resistivity data has been used effectively in detecting liquid waste (Daily et al, 2004; Ramirez et al., 1996), in saline tracer tests (Perri et al., 2012; Kemna et al., 2002; Monego et al., 2010), and in model calibration at a field site for a controlled tracer test (Binley et al., 2002a). In recent studies, time-lapse electrical resistivity data have been used in quantifying the spatiotemporal distribution of contaminant concentration (Gasperikova et al., 2012; Kowalsky et al., 2011).

The previous studies shows well the usefulness of the measure of electrical resistivity in monitoring solute distribution. However, as many have mentioned in their

studies, the efficiency of geophysical data is somewhat dependent on the auxiliary information on groundwater level and groundwater quality from in situ observation.

At the field site of our study, there are hardly any alternative methods to collect data other than electrical resistivity survey, while it is very limited to collect hydrogeological and geochemical data to support the geophysical data.

Thus the objective of this study is to suggest a method to use electrical resistivity data effectively, even with insufficient auxiliary data. Since the resistivity data is displayed as images, we analyzed the property of the images and compared it with a visual display from the result of the numerical simulation. The similarity between those images were evaluated quantitatively, thus the simulation model could be validated with increased accuracy in prediction of leachate transport.

3.2 Site Description

The first outbreak of Foot-and-mouth disease in Korea was occurred in November 2010 and spread all over the country. To combat the highly communicable disease the government had vaccinated the livestock across the country and had culled roughly 10 percent of the country's pigs and cattle population (Ramstad and Woo, 2011; Wong, 2011). The mass cull resulted in more than 4600 of burial site all over the country.

The burial site of this study is located on a gentle hill slope in Icheon, Korea, and the down slope of the area is an agricultural area (Figure 3.1). The geology was mainly composed of igneous rock of unknown age with intrusive granite of the Jurassic period, then of igneous rocks and dikes of the Cretaceous which are overlain by the quaternary alluvium of the Cenozoic period (MOLIT and K-water, 2011).

Figure 3.1 Map of study site in Icheon and location of burial pits.

Two burials, 10×10×5 m (length×width×depth) in dimension each, were located along the slope of the site. The interior bottom and side of the burial pit was regulated to be lined with bentonite mixture which has very low permeability and with impermeable cloths to hamper leachate produced during the decomposition to leak out from the pit into groundwater nearby. After the burial, soil layer covered the pits and its top was covered with impermeable cloths. Vent pipes were built to allow gas to transfer out of the pits and a monitoring well was set up to monitor leachate leakage. Location of the burial pit was regulated to be at a distance from groundwater wells, streams supplying domestic water usage, and residential district to minimize the influence of possible leachate from the burial. At the burial site of this study, about 5,000 head of pigs were buried in January of 2011.

The hydraulic conductivity of the burial site was measured using a monitoring well next to the burial pit and the result showed that the hydraulic conductivity of the top 10 meter-depth layer is approximately 1×10^{-4} m/s which corresponds to well-sorted sand (KIGAM, 2012).

The amount of rainfall in the study area was 1370.9 mm in 2011, and due to the highly intensive rainfall during summer in Korea, 73 % of the total rainfall of 2011 was concentrated between June and August (Figure 3.2).

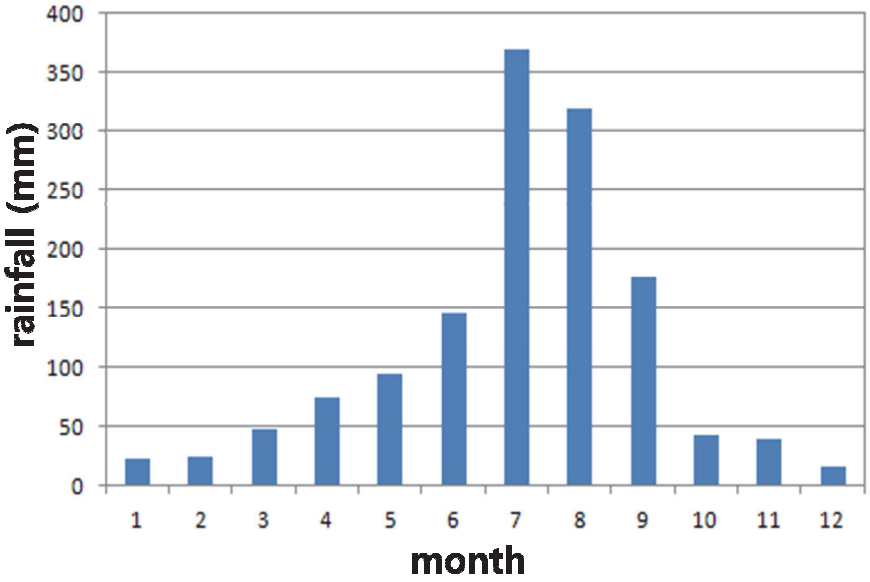

Figure 3.2 Monthly rainfalls of 2011 of Icheon (www.kma.go.kr)

3.3 Methods

3.3.1 Electrical resistivity survey

The electrical resistivity of subsurface depends on the solid and fluid constituents and on their spatial and temporal variations. Thus the measure of the electrical resistivity can assist in elucidation of unknown geophysical properties i.e. geological formation, fluid saturation, or contaminant concentration. To measure the electrical resistivity, an electric current is introduced directly into the ground through electrodes and the electrical resistance is obtained from the voltage measurements by applying Ohm's law:

$$E = \rho J \text{ or } J = \sigma E \qquad [3\text{-}1]$$

where E is the electric field in volts per meter (V/m), J is the current density in amperes per square meter (A/m^2), ρ is the resistivity in Ohm-meters (Ω-m) and σ is the electrical conductivity in siemens per meter (S/m). Electrical conductivity is a measure of a material's ability to conduct an electric current.

Electrical resistivity methods use an array of electrodes to measure the subsurface resistivity. A known current is injected between two electrodes and the potential difference is measured across other two electrodes on the survey line. There are several different types of electrode array and the dipole-dipole array, which is especially good

for depth penetration and sensitive to vertical resistivity boundaries with high resolution.

In the dipole-dipole array, the potential gradient is over a closely spaced electrode pair, while a pair of the current electrode is located outside of the potential electrodes. The separation between both pairs of electrodes should be the same L, then the separation between the centers of the dipoles is restricted to L(n+1). The apparent resistivity is given as follows:

$$\rho_a = \pi \mathrm{Ln}(n+1)(n+2)\frac{\Delta V}{I} \qquad [3\text{-}2]$$

where ρ_a is the apparent resistivity of the medium, n is the total number of electrodes, I is the current at the current electrodes and ΔV is the voltage between the potential electrodes.

In this study, total of eight surface electrical survey lines were set up around the burial pits and collected data at different times in order to see the temporal distribution of the leachate (Figure 3.3). To find out temporal and seasonal variation of the leachate distribution, surface lines were set up and measured the electrical resistivity in June, August, and December. The measurements during June were performed repeatedly with several time lapses. With this approach, the effects of geological heterogeneity can be removed while the temporal changes in solute distribution are emphasized.

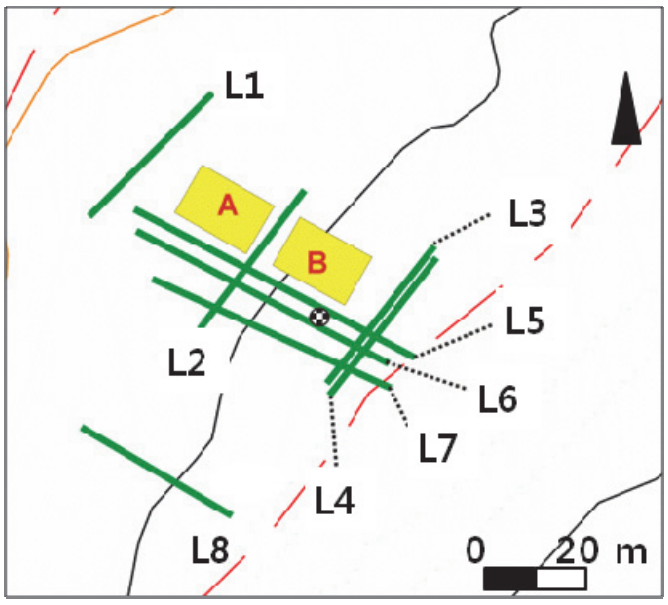

Figure 3.3 Map of burial pits survey lines. Two burial pits are represented as yellow box. The upper pit is labeled A and the lower pit B. The eight electrical resistivity survey lines are in green solid line with its name (L1 – L8).

3.3.2 Simulation of leachate transport

HydroGeoSphere (Therrien et al., 2005), a three-dimensional numerical model describing variably saturated subsurface flow and solute transport is used for simulation of leachate transport from the burial pits. A conceptual model is set up to simulate the groundwater flow of the region and the transport of leachate which is assumed to come out from the burials. Model domain was bounded by a stream and hill ridges surrounding the burials (Figure 3.4). The hydrogeologic unit of the model domain was built to have five different layers (Figure 3.5) and the property of each layer is given in Table 3.1. A finite element triangular mesh was used for the model domain and appropriate meshes were generated corresponding to the geometries of burial pits and topography of the modeled area (Figure 3.4). The final domain consists of 10 layers which comprises 5 different materials. The number of nodes and elements are 11,671 and 20,120, respectively. To describe the lining at the bottom of the pits, very low value of hydraulic conductivity is assigned for the corresponding meshes.

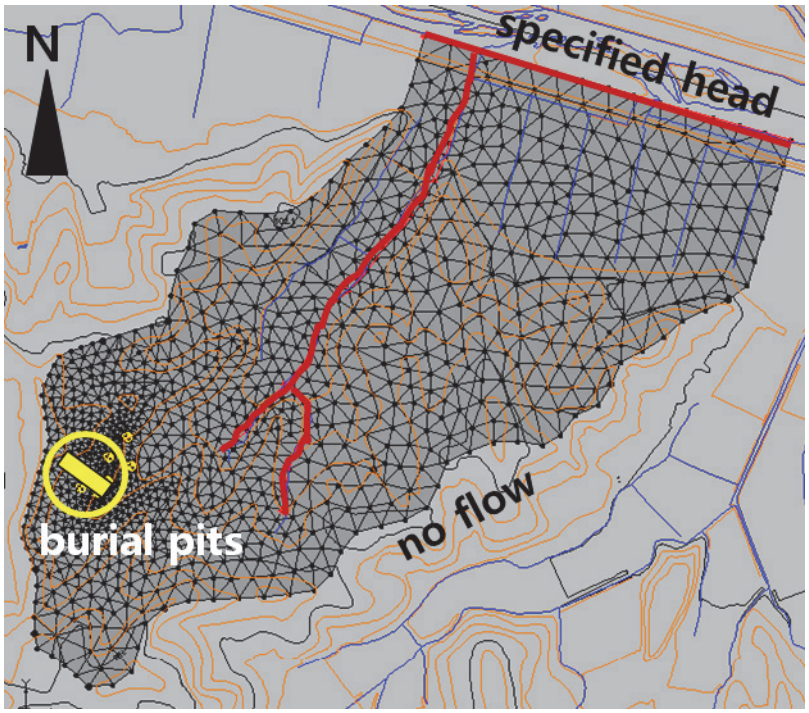

Figure 3.4 Model boundary and burial locations in the model domain. Triangular mesh of the top surface is also shown in the map.

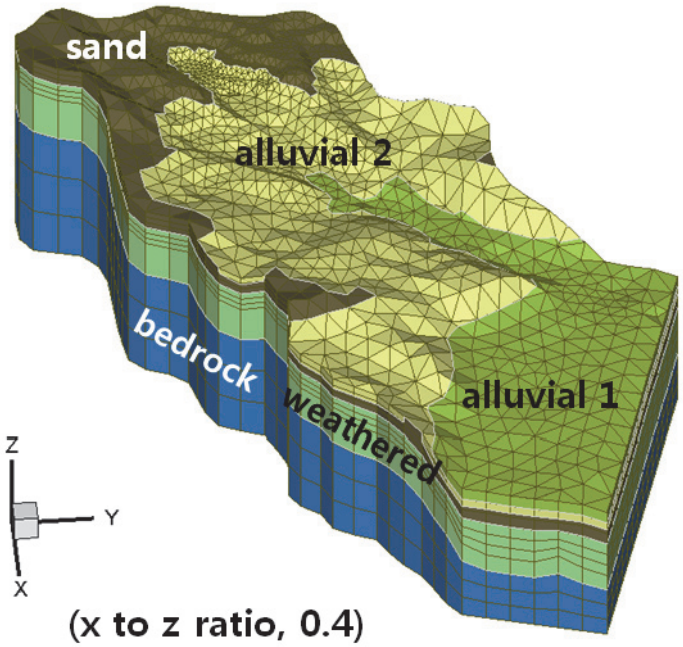

Figure 3.5 Five layers constituting the model domain. Hydrogeologic properties of each layer are given in Table 3.1.

Table 3.1 Hydrogeologic properties used as input for model simulation

	Alluvial 1	**Alluvial 2**	**Sand**	**Weathered rock**	**Bedrock**	**Lining**
K_x, K_y	200	4	0.27	0.0025	0.00003	0.00001
K_z	20	0.4	0.03	0.0006	0.00003	0.00001
Porosity [-]	0.35	0.3	0.3	0.2	0.05	0.02
Dispersivity [m]						
α_L				10		
α_T				1		
Tortuosity [-]				0.1		

* K in [m d^{-1}]

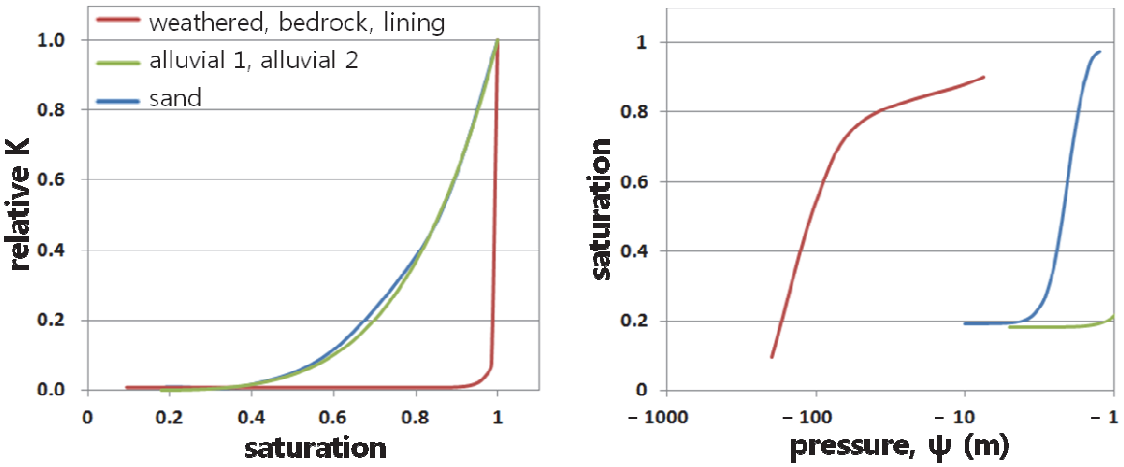

Figure 3.6 Relationships of saturation-relative permeability and pressure-saturation of each material for variably-saturated simulation

For simulating variably saturated flow, the relation between the pressure head, saturation and relative permeability is required. Figure 3.6 shows these relationships used in the simulation of this study which refer to Therrien et al. (2005). Along the stream boundary, specified head is assigned throughout the simulation time of 10 years and along the hill ridges, no flow boundary conditions is assigned (Figure 3.4). The monthly rainfall is assigned on the top surface of the model domain following the data given by Korea Meteorological Administration (Figure 3.2) and 15 % of the rainfall was assumed to be recharged into the aquifer.

Since the interest of this study is to understand the possible distribution and transport pattern of leachate from the burial pits in case there is leakage of the leachate, the burial pits were assumed as the contaminant source that produces approximately 2500 kg of ammonium in total for the time period of three years after the burial event. Reactive transport of solute is beyond the scope of this study, and no reaction is considered for the ammonium which is assumed as the source of contamination released at the burial pits in the model.

3.3.3 Image similarity metric

Image comparison approach is used in this study to validate the model adequacy. The distribution of electrical resistivity on 2-dimensional vertical section along a survey line is compared with the distribution of leachate concentration from the simulation result on the identical section. The Euclidean distance approach is applied when comparing the image similarity between the resistivity measurements and simulation results.

The Euclidean distance is the length of the line segment between two points p and q. If p=(p_1, p_2, ..., p_n) and q=(q_1, q_2, ..., q_n), then the distance between p and q is given as follows:

$$d^2(p,q) = \sum_{i=1}^{n}(p_i - q_i)^2 \qquad [3\text{-}3]$$

When measuring distance between images, the color levels of corresponding pixels of each image in a raster format can be employed ad p_i and q_i.

However, small deformation in the image can result in huge distance value, since the distance measure following the equation above does not consider the spatial relationships of pixels. Thus, Wang et al. (2005) proposed an image Euclidean distance (IMED) method, which takes the spatial relationship of image pixels into account and is robust to both noise and small deformation. The IMED between images x and y is

defined as

$$d_{IE}^2(x,y) = \sum_{i,j=1}^{MN} g_{i,j}\,(x_i - y_i)(x_j - y_j) = (x_i - y_i)^T G(x_j - y_j) \quad [3\text{-}4]$$

where x_i and y_i are the color level at the ith pixel, p_i, the symmetric and positive definite matrix G is metric matrix, and g_{ij} is the metric coefficient indicating the spatial relationship between pixels p_i and p_j. The definition of g_{ij} is given by

$$g_{ij} = \frac{1}{2\pi\sigma^2} \exp\left(-\frac{(d_{ij}^s)^2}{2\sigma^2}\right) \quad [3\text{-}5]$$

where d^s_{ij} is the spatial distance between p_i and p_j on the image lattice, and σ is the width parameter (Li and Lu, 2009; Wang et al., 2005).

In this study, rasterized images from the resistivity distribution and the concentration contour on an identical section are compared with the IMED approach to quantify the validity of the simulation result.

3.4 Results and Discussion

3.4.1 Electric resistivity near the burial pits

The 2-dimensional electrical resistivity distributions recovered from the measurements are shown in Figure 3.7, 3.8, 3.9, and 3.10. Survey line L1, and L8 are measured in order to collect information about background resistivity of the area excluding the possible influence of leachate (Figure 3.7). The vertical resistivity

distribution along L1 and L8 shows that the layer of high resistivity exists in the upper layer. Since the electrical resistivity in the background area of the burial pits is rather high, one can detect the leachate leakage which would have low electrical resistivity value without difficulties.

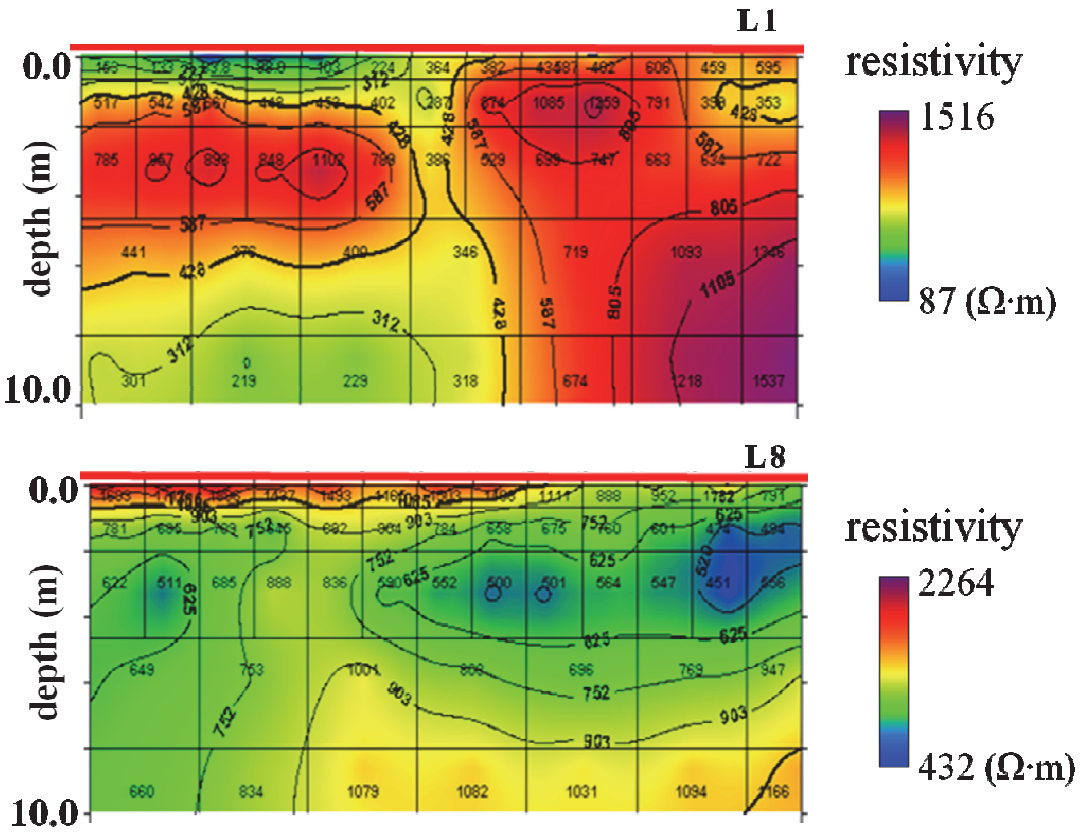

Figure 3.7 The distribution of electrical resistivity measured along the survey line L1 and L8 on June 5th.

L3 and L4 are located at the down gradient of the lower burial pit. It is apparent in Figure 3.8 that there is a zone of low resistivity below the location of the lower burial pit, and thus the low conductivity zone can be supposed as leachate leakage. All the burials constructed in 2011 to hamper the contagious disease were supposed to be lined carefully to prevent the possible leakage of leachate from the decomposition; however some amount of leachate seemed to seep out from the burial pit at this site. When the resistivity distribution of L3 and L4 are compared, one can notice the spatial differences in leachate distribution. As L4 was aligned with L3 with 2 m distance in the direction further from the lower burial pit, it seems that the leachate is still distributed near the source even about 5 months after the burial event.

The zone of low resistivity is also shown along the L2 line which is located at the down gradient of the upper burial pit (Figure 3.9). The leachate is distributed more to the left side of the burial pit, where a groundwater well is located to monitor leachate leakage. An increase in subsurface connectivity or a disturbance due to the well can be a reason of the left-sided leachate distribution.

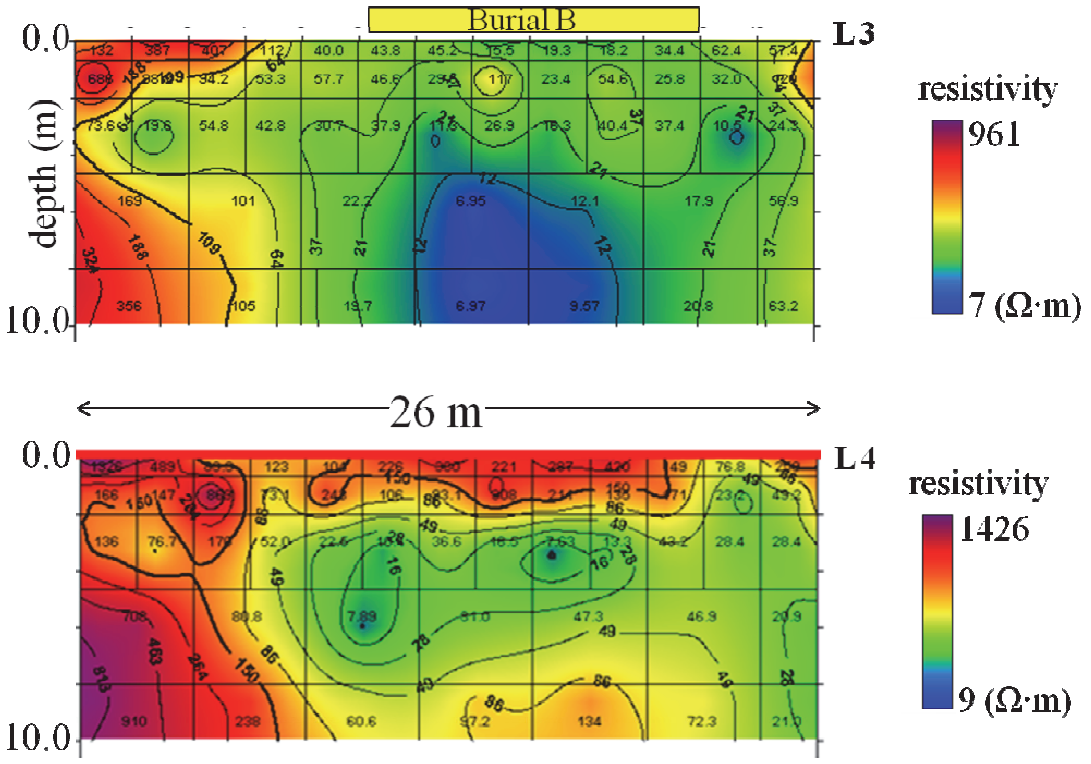

Figure 3.8 The distribution of electrical resistivity measured on June 5th along the survey line L3 and L4 which are located right down gradient of the lower burial pit, B.

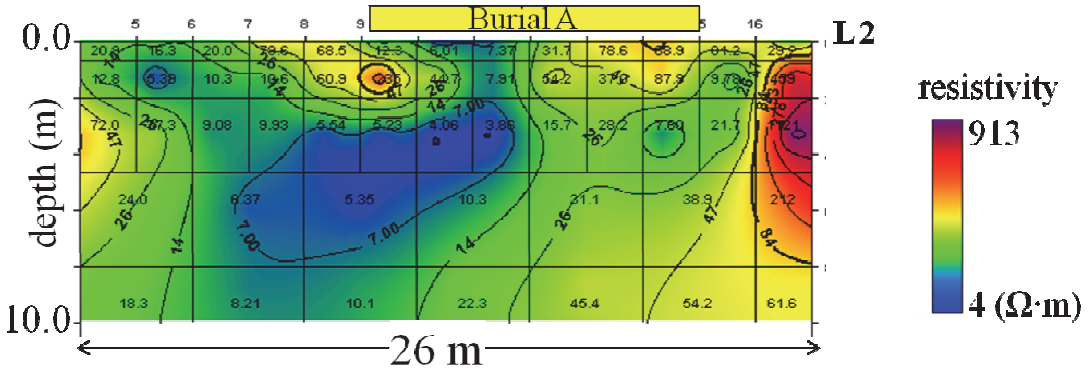

Figure 3.9 The distribution of electrical resistivity measured on June 6th along the survey line L2 which are located at the down gradient of the upper burial pit, A.

The resistivity measured at different time shows the temporal transport of the leachate. In Figure 3.10, the leachate distributions at the vertical section of L3 measured in June, August, and December is shown. Vertical distribution of low resistivity zone in June has changed to have horizontal distribution in later times. The change in the pattern of distribution could have been caused by seasonal variation or by temporal weather event. However, one can tell that there is still leachate leaking from the burial until almost a year after the burial event but its concentration and extent seem to be decreased in December.

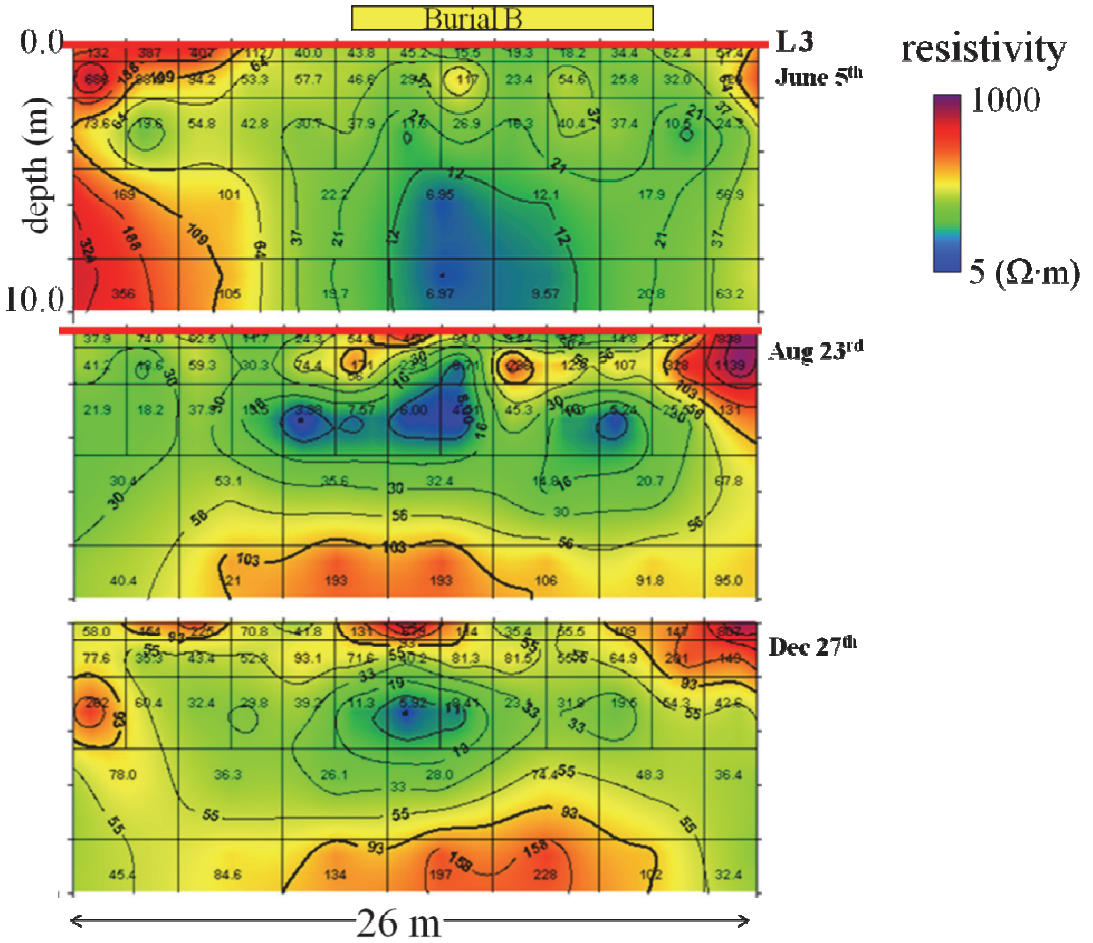

Figure 3.10 Temporal distribution of the electrical resistivity at the vertical section of L3 on June 5th, August 23rd, and December 27th of 2011.

3.4.2 Leachate transport from the burial

The simulation result shows that the groundwater in the region flows from the hill ridges of the highest elevation on the southern boundary toward the small valley in the center, then to the stream on the northern boundary (Figure 3.11). As the recharge boundary is given on the top surface referring the rainfall data of Icheon in 2011. The groundwater level in the domain is elevated during the summer season and decreased during the winter season. Calibration of the model for hydraulic head was unattainable since only one well which was built to monitor the leachate leakage was available for the measurement of groundwater level in the modeled area. When the groundwater level observed at the monitoring well is compared with the simulated groundwater level at the same location, the pattern of the level change throughout the year shows similarity, but there was some differences especially in summer season. The local groundwater flow direction near the burials is shown in Figure 3.11. Since the topography of the location of burials has somewhat steep slope, groundwater is simulated to flow from the upper pits to the lower pits, and then to the northern stream boundary.

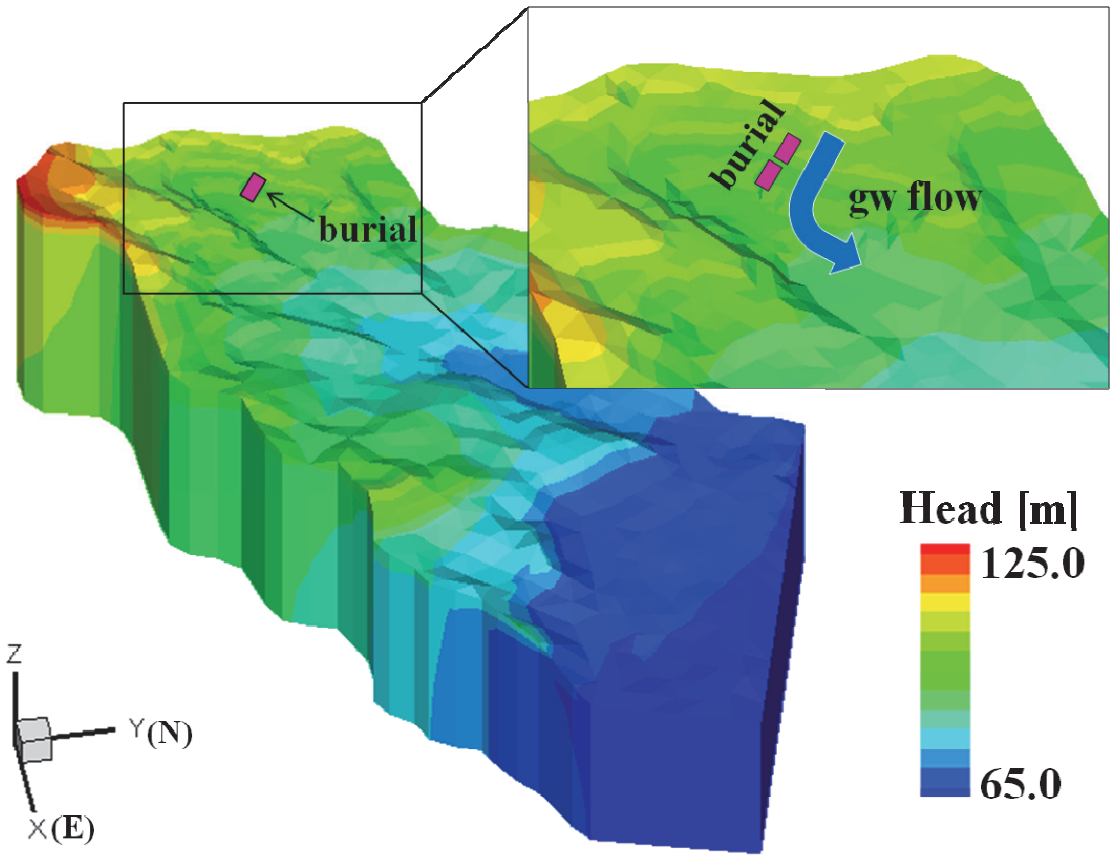

Figure 3.11 Initial hydraulic head distribution in the model domain from the simulation result.

As described earlier, the burial pits are modeled as contaminant source. Distributions of ammonium at different times are shown in Figure 3.12. Concentration distribution on a vertical section AA′ is shown in the Figure. The white solid lines lying horizontally in the vertical section show the water table level. A great portion of the contaminant seems to move mainly through the unsaturated zone, but still the plume of low concentration extends to saturated area even until 3 year after the start of the simulation. The simulation results show that if the leachate is discharged from the burials, its influence would continue for several years after the burial event, leading to deterioration of aquifer and groundwater in the neighborhood.

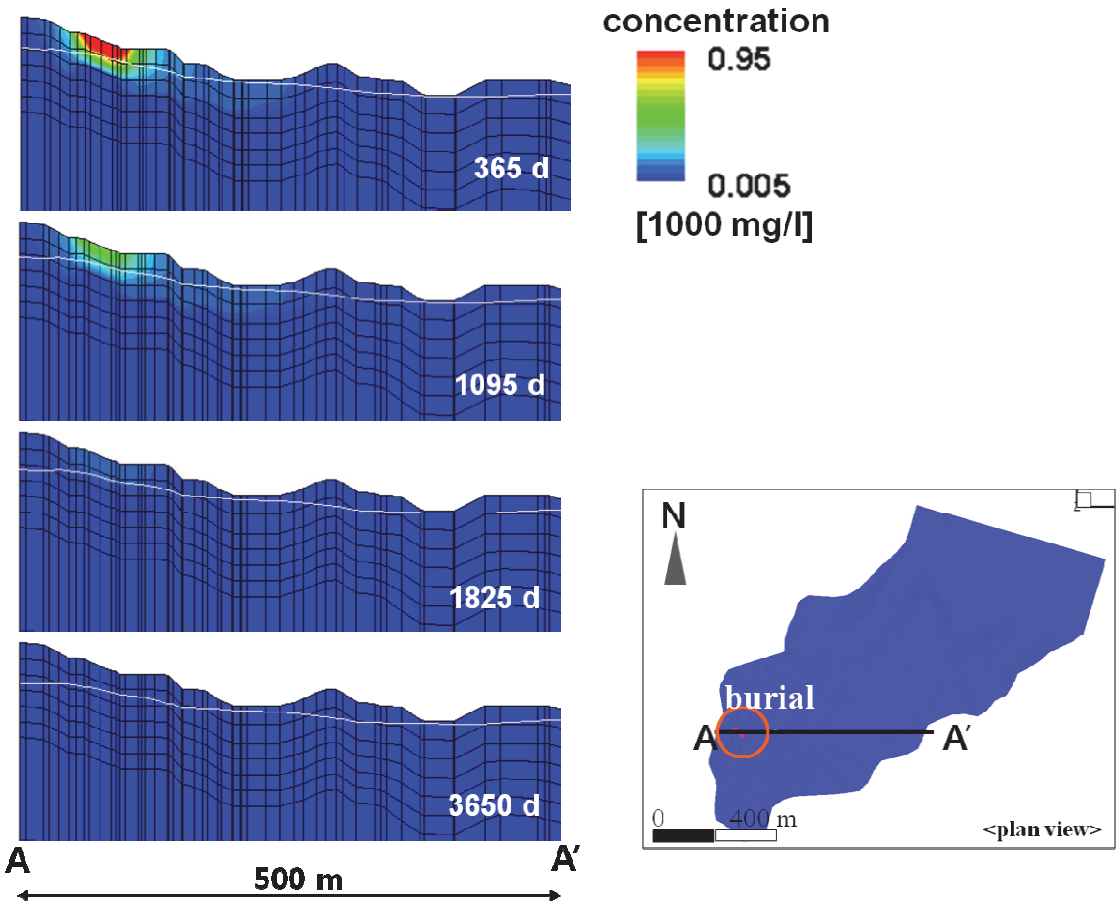

Figure 3.12 Temporal distribution of ammonium on the vertical section of AA' at time 365, 1095, 1825, and 3650 day after the start of simulation. Ammonium is assumed to leak from the burial pits in the simulation model.

3.4.3 Image similarity: IMED

To utilize the simulation result in setting up a strategy to protect groundwater quality near the burials, the model results need to be validated. The image Euclidean distance method is employed for this purpose. Figure 3.13 is a vertical section of concentration distribution along a line that corresponds to the electrical resistivity survey line, L2. The section shows the concentration distribution at 120 day after the start of simulation, which roughly equivalent to the time of measurement of the electrical resistivity in June considering the burial is constructed in January.

Rater data of the images in Figure 3.9 and Figure 3.13 are extracted and the Euclidean distance is calculated. Concentration contour in the area that corresponds to the section where the result of resistivity measurement is available is chosen for calculating image distance. In computing Euclidean distance between two images from the electrical resistivity measurement and the leachate transport simulation, the electrical resistivity value and the leachate concentration value are used as the substitutes for the color index. The both values are normalized to make them have the same scale for reasonable analysis.

The Euclidean distance between the two images along L2 is computed to be 3.5

when the spatial relation between pixels is not considered, however the image Euclidean distance (IMED) which considers the spatial relations is 1.4. The result shows that the two images are close each other especially when the spatial relation is considered. The results of IMED calculation for other sections are given in Table 3.2. The electrical resistivity measurement results of June, August and December are compared with the simulation results at 120, 181, and 304 day of elapsed time after the start of simulation, respectively, and their IMED and the Euclidean distance values are also shown in the table.

The IMEDs are in the range of between 1.27 and 2.46 showing consistency in the relationship of the two images resulting from the field measurement and simulation. The distance variation along time doesn't seem to be increased while there is some variation along different section. The larger IMED value on L5 and L6 is supposedly considered as the result of heterogeneity of the location. The model validation can be improved by reducing the distance value of IMED result.

Since the simulation results seems to represent the leachate transport in the study site as a whole, Figure 3.3 implies that the influence of the leachate can be extended to hundreds of meters down-gradient of the burial even after 3 year since the burial event.

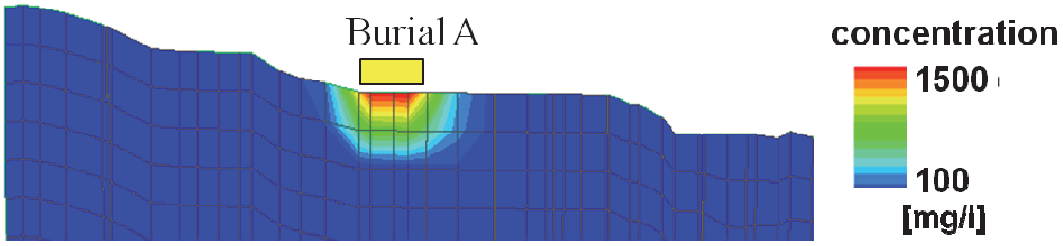

Figure 3.13 A vertical section of concentration distribution along a line equivalent to L2 at time of 120 day after the simulation, which roughly corresponds to the time of measurement in June. The yellow box in the figure shows the location of the upper burial pit.

Table 3.2 The IMED and Euclidean distance values between electrical resistivity measurement results of June, August and December and the simulation results at 120, 181, and 304 day of elapsed time after the start of simulation.

Cross section	Date of measurement (2011)	Elapsed time of simulation [day]	IMED	Euclidean distance
L2	06-Jun	120	1.39	3.50
	23-Aug	181	1.95	4.57
	27-Dec	304	1.77	3.68
L3	05-Jun	120	2.13	5.31
	06-Jun	120	1.81	4.51
	10-Jun	120	1.98	4.93
	23-Aug	181	1.27	3.17
	27-Dec	304	1.65	4.23
L4	05-Jun	120	1.37	3.39
	27-Dec	304	1.93	4.59
L5	06-Jun	120	2.36	5.56
	09-Jun	120	2.46	6.14
L6	05-Jun	120	2.28	5.54
L7	06-Jun	120	1.63	4.16
	10-Jun	120	1.60	4.12

3.5 Conclusion

This study suggests a method to use electrical resistivity data effectively, even with insufficient additional data when validating a simulation model for site description and analysis. Since the resistivity data is displayed as images, we analyzed the property of the images and compared it with a visual display from the result of numerical simulation.

For a carcass disposal site in Icheon which is constructed during the outbreak of the Foot-and-mouth disease in 2011, possibility of leachate leakage from the burial needed to be analyzed. A simulation model is set up to describe leachate transport in the site; however there are hardly any methods to collect data for model calibration and validation.

Thus, the surface electrical resistivity is measured along eight survey lines around the burial pits. The survey results show that leachate is leaked from the burial pit and continued to migrate and dispersed until a year after since the time of burial. In the simulation model, the burial pits are assigned as contaminant source and the groundwater level seem to be in agreement with the observation at the only well next to the burial. Since the simulation model lacks validation just with one well data, image similarity metric is employed.

When the images of the resistivity distribution the concentration distribution on the same vertical section along L2 at the same time period, the Euclidean distance and IMED is computed to be 3.5 and 1.4 respectively.

The result suggest that the simple image similarity metric can be used efficiently in validation of model and the quantitative evaluation of simulation result can help to improve the accuracy in prediction using the model.

Chapter 4 Hydrogeochemical analysis of salinity in groundwater in a coastal environment

Abstract

Seawater intrusion can be activated by the construction of underground caverns which act as groundwater sinks near a coastal area. In an environment complicated with such artificial structures, seawater intrusion is not simple and thus needs to be evaluated by means of multiple analytical approaches. This study uses geochemical and isotopic indicators to assess the characteristics of salinized seepage into an underground oil storage cavern in Yeosu, Korea. Cl^-/Br^- ratios, principal component analysis (PCA) of chemical data, and stable isotope data were used to determine the origin and the extent of salinization. Indications of seawater intrusion into the cavern through fractured bedrocks were observed; however, it was highly probable that another source may have contributed to the observed salinity. The PCA results revealed that the seepage water chemistry was predominantly affected both by seawater mixing and cement material dissolution. The maximum seawater mixing ratio in the seepage water was estimated on the basis of the Cl^-–Br^- mixing ratio and the Cl^-–$\delta^{18}O$ relation, with the results showing considerable variation ranging from less than 1% to as high as 14%, depending on the

cavern location. The spatial variations in the chemical characteristics and in mixing ratios are believed to have resulted from the hydrogeological heterogeneity of the study site, as caused by both fractured aquifer and the cavern facilities.

4.1 Introduction

A coastal aquifer is vulnerable to seawater intrusion because a small drawdown in groundwater head may cause a significant shift of the seawater–freshwater interface. An underground cavern with unlined walls, which allow groundwater seepage into the cavern, is a typical example of a groundwater sink that may shift the seawater–freshwater interface. At an underground oil and gas storage facility, preventing the leakage of gas and oil from the storage cavern is an important problem. To avoid this type of leakage, the groundwater pressure must be higher than the interior gas pressure in the cavern (Kim et al., 2000; KNOC, 2010). This condition can be ensured by means of a water curtain system which injects water into the cavern. The injected water and groundwater around the cavern flows through fractures in the bedrock into the cavern, eventually collecting as seepage water at the bottom of the cavern and sinking due to the density difference between the oil and the water (Figure 4.1). The seepage water mixes with the adjacent groundwater; thus, the chemical composition of the seepage water flowing into the cavern may reflect the chemical composition of groundwater near the cavern as a result of the interaction between the water and the surrounding fractured crystalline rocks.

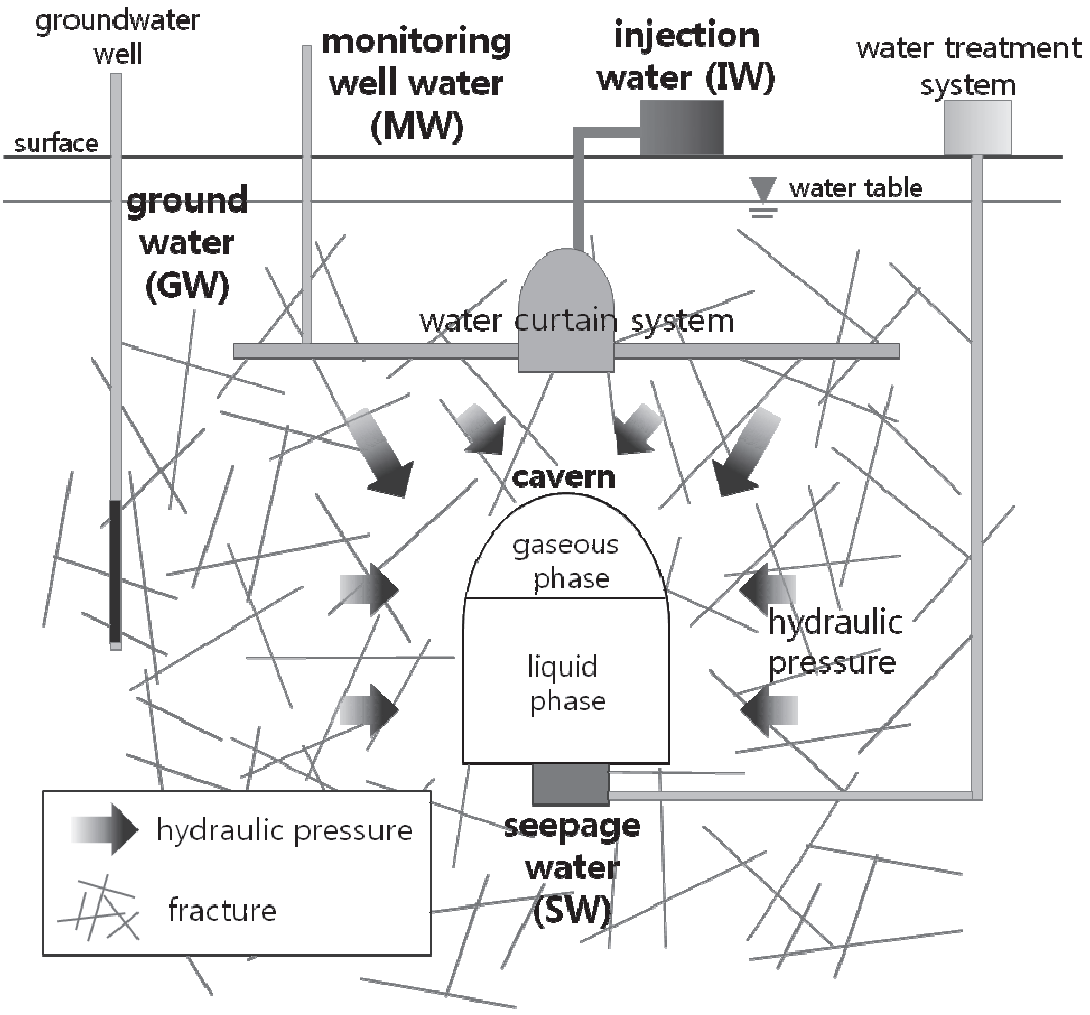

Figure 4.1 A schematic illustration of structure of an underground oil storage cavern. Types of water sample - injection water, monitoring well water, groundwater, and seepage water - are also shown (Lim et al., 2013).

There are some concerns which may occur during the operation of cavern facilities. The chemistry of groundwater and seepage water around a storage cavern can be changed by the influence of numerous factors. The groundwater chemistry near a storage cavern system can be altered artificially by disinfectant injections such as sodium hypochlorite (NaOCl) or through the use of cement materials in the inside wall of a cavern, built to ensure stability (Lee et al., 2007; 2008). Additionally, groundwater from an underground storage cavern near a coastal area can be salinized by seawater intrusion (Kim et al., 2003; Lee et al., 2007; KNOC, 2010). Lee et al. (2007) reported that three hydrogeochemical events, namely, encrusted cement dissolution, host rock dissolution, and seawater intrusion, may have influenced the groundwater quality of a storage cavern site that they studied. The hydraulic conditions are also can be changed by various causes. Both the hydraulic head and seepage rate in an underground liquefied petroleum gas (LPG) storage cavern reportedly decrease presumably due to biological clogging (Geostock, 1992; Chang and Lee, 1998). On the other hand, Kim et al. (2000) demonstrated that sudden changes in the seepage rate and hydraulic head were mainly caused by changes in the operation conditions, but not biological clogging. These chemical and physical changes in groundwater and seepage water around a storage cavern may deteriorate the petroleum stored in the cavern, corrode the storage facilities,

and cause the leakage of gas and oil from the storage cavern.

To avoid unexpected operational problems and to ensure the long-term operation of these types of caverns, the groundwater flow system and the water quality have been under close monitoring since the construction of the underground caverns of interest in this study (KNOC, 2010). The Yeosu underground oil storage cavern complex, which was the target area of this study, is located in a coastal area in southern Korea. It has an unusually high concentration of ions in its seepage water, especially sodium (Na^+) and chloride (Cl^-). As mentioned earlier, high salinity can be a threat to a long-term operation of a storage cavern. Thus, identifying the origin of salinity and estimating quantitatively the extent of its mixing should be prioritized to ensure the stable operation of these caverns.

The objective of this study is to investigate the origins and inflow routes of salinity of the seepage water and to assess the extent of the seawater intrusion. Ion ratio analysis, multivariate statistical analysis (Principal Components Analysis), and stable isotope analysis were combined with hydrogeological observations for the interpretation of saline water transport.

4.2 Site description

The study site is a hilly area in Yeosu, located at the southern coast of the Korean peninsula (Figure 4.2a). The area is mainly composed of Mesozoic volcanic rocks of tuff and andesite, overlain by intrusive granite of the late Cretaceous period. This bedrock is composed of compact and solid rock except in fracture zones and at interfaces with intrusive granite. A local major fracture zone, F1-1, exists in the NE direction along with numerous small-scale fracture zones around the storage caverns, which increase the hydrogeological heterogeneity of the study site. The mean hydraulic conductivity of the rock mass is reported to be in the range between 1.0×10^{-9} and 1.0×10^{-8} m s^{-1}. The hydraulic conductivity of fracture zones in the region vary widely from 5.0×10^{-11} to 5.0×10^{-7} m s^{-1}, and leakages through fracture zones with high permeability have been observed (KNOC, 2010). The surface soil, with approximate hydraulic conductivity of 1.0×10^{-7} m s^{-1}, is developed with a thickness of 0.3–10.5 m which varies with the topography of the area.

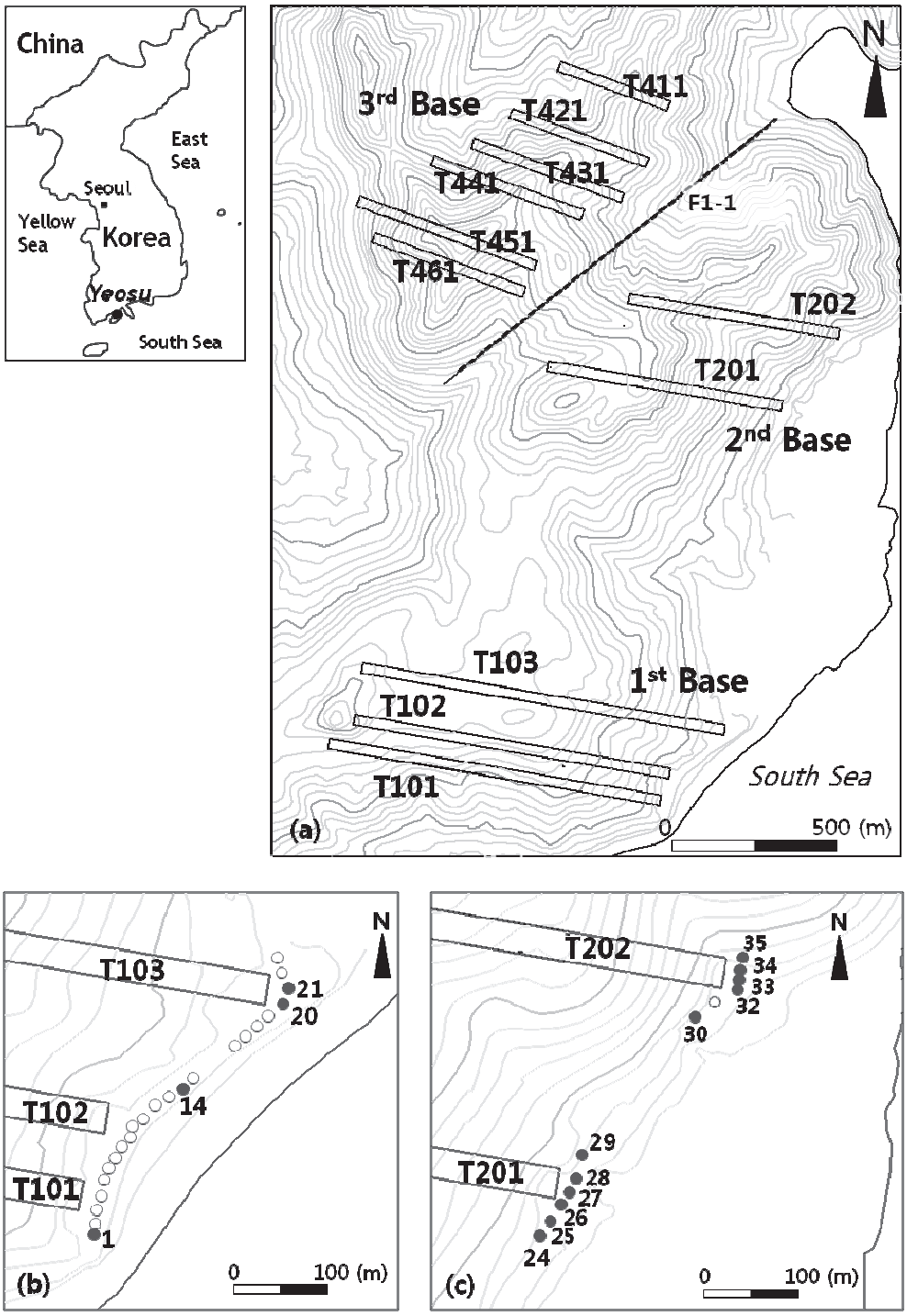

Figure 4.2 Location of (a) Yeosu storage complex and the name of each cavern composing each storage base. Each cavern is represented as a rectangular. Open and solid circles in (b) and (c) are seawater intrusion barrier wells at the frontage of (b) the 1st and (c) the 2nd storage bases. Numbered circles are the wells where measurements were available and the numbers represent their name.

The hills in the study area range in height from 200 to 340 m, with steep slopes on their eastern faces. The hydraulic gradient in the area also has a steep slope from the hill ridges to the coast on the eastern side due to the topographic features of the area. Rainfall is mostly discharged as surface runoff due to thin soil layers and limited storability of the fracture zones (KNOC, 2010). A numerical simulation by Lee et al. (2012), as calibrated using the long-term monitoring data of hydraulic heads and the cavern operation pressures, showed regional groundwater flow from the western hill ridges to the eastern coast with a local sudden drop of the hydraulic head at the cavern area. More detailed descriptions of the geology and hydrogeology of the study site were presented by Lee et al. (2012), who focused on the numerical modeling of the study site.

The storage facility in this area is located under the ridges of the hills. There are three storage bases (Figure 4.2a) that were built over two time periods; the 1st and the 2nd bases have been operating since 1998 and the 3rd base since 2009. The 1st base comprises three caverns, termed T101, T102, and T103. The 2nd base comprises two caverns, T201 and T202. The 3rd base has six caverns: T411, T421, T431, T441, T451, and T461 (Figure 4.2a). The height of the storage caverns is 30 m, and the base of each cavern is located 60 m below sea level. The length of the cavern in the study site is different for each cavern raging from 630 m to 1730 m. The underground cavern system

has an access tunnel, water curtain tunnels, water curtain boreholes, and storage caverns. More than 50 groundwater observation wells are located near those caverns, and have been under hydraulic head monitoring since 1999 to monitor the tightness of the storage system. Most of those wells reach -30 m (AMSL), the depth of the cavern top, although well depths vary widely from -70 to 10 m (AMSL). Pressure head at the top of the cavern during the operation was kept to be 3 m approximately, which is lower than the groundwater head of the surrounding area.

Seawater intrusion barrier wells with a depth of 85–100 m are installed additionally at the front of the 1st and the 2nd storage bases in order to prevent seawater intrusion into the caverns by injecting fresh water into the wells (Figures. 4.2b and 4.2c). The average screened interval extends from -30 to -80 m above mean sea level (AMSL), through which fresh water is continuously injected; the mean water injection rate is 4.0 m^3 day^{-1} for each well.

4.3 Methods

4.3.1 Sampling and analysis

Various water samples from 47 points in the cavern site have been collected to monitor the physical and chemical characteristics of the water since 1999 (KNOC,

2010); samples include injection water (IW), monitoring well water (MW), water in tunnels (WT), seepage water (SW), and groundwater (GW). Injection water is water that is injected into the water curtain system to add pressure to the caverns. Monitoring well water refers to the water in the water curtain system. The water in the access tunnel, which was built during the excavation of the caverns, is referred to as water in tunnels. Seepage water is the water which collects at the bottom of the cavern (Figure. 4.1). The monitoring of IW, MW, WT, and SW started in 1999; water sampling and analysis were performed twice a year biennially from 2000 to 2008, and then annually since 2009. Sampling GW started in 2008, and is performed selectively at certain wells, which may not be identical every year. GW wells are shown in Figure 4.3a as circles; solid circles represent wells where samples have been analyzed for water quality.

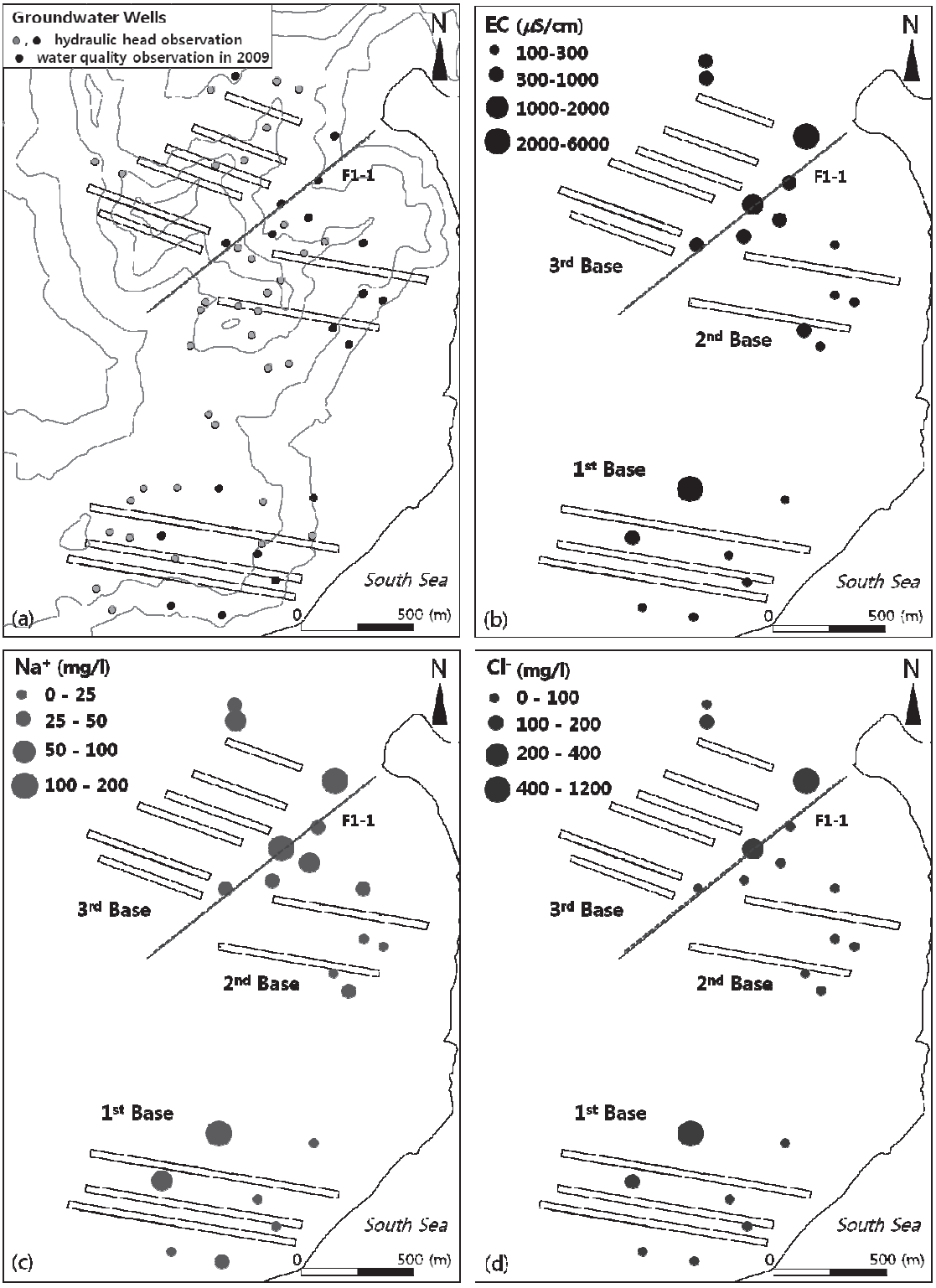

Figure 4.3 (a) Location of groundwater well near the caverns and the value of (b) EC, (c) Na^+, and (d) Cl^- at those wells plotted on the local map.

Water samples from the seawater intrusion barrier wells were collected at multi-level depth in 2010 to investigate if seawater invades from the coastline. The water injection process to those barrier wells was halted for more than a week prior to the sampling.

Temperature, pH, redox potential (E_h), electrical conductivity (EC), and dissolved oxygen (DO) were directly measured at each sampling point. Alkalinity was also determined using Gran titration method (Stumm and Morgan, 1996). Cation and anion concentrations were analyzed using ICP (inductively coupled plasma atomic emission spectrometer) and IC (ion chromatography), respectively.

Water samples from SW and the seawater intrusion barrier wells were collected for hydrogen and oxygen isotope analyses to investigate the potential for seawater intrusion. The stable isotope analysis was performed at Korea Basic Science Institute (KBSI) using a GV Instrument mass spectrometer. Oxygen isotopes were measured following the H_2O-CO_2 equilibrium method developed by Epstein and Mayeda (1953) and hydrogen isotopes were measured using the chromium reduction technique developed by Morrison et al. (2001). The samples were measured repeatedly with precision levels of ±0.1‰ and ±1.0‰ for $\delta^{18}O$ and $\delta^{2}H$, respectively.

4.3.2 Data analysis

Ion ratios, particularly chloride (Cl^-) and bromide (Br^-) ratios were examined to identify the origin of the salinity in high-Cl^- water samples. Cl^- and Br^- ions exist in all natural water and are good tracers due to their conservative behavior (Davis et al., 1998; 2004). The Cl^-/Br^- ratio has been shown to be an effective index to identify the origin of chloride in groundwater, as most physical processes may change the absolute concentrations but not modify the ion ratio of its origin (Sánchez-Martos et al., 2002; Demirel, 2004; Panno et al., 2006; Alcalá and Custodio, 2008). The Cl^-/Br^- molar ratio of seawater is known to be uniform around 655±4 (Davis et al., 1998) with a Cl^- concentration of about 19,000 mg l^{-1}.

The multivariate statistical method known as principal component analysis (PCA) was used to determine the hydrogeochemical features and the origin of the salinity of the underground storage cavern complex in the coastal area. PCA is a useful method to uncover patterns in data with a large number of variables (Morell et al., 1996; Lee et al., 2007). It compresses the data by means of artificial variables called principal components (PCs), which are linear combinations of weighted original variables. Principal components account for most of the variance in these variables; thus, they retain most of the information contained in the original variables. SAS 9.2 package

(SAS Institute Inc., 2009) was used in this study for the PCA. The variables used in the analysis were pH and concentrations of Na^+, K^+, Ca^{2+}, Mg^{2+}, Si, Cl^-, SO_4^{2-}, and HCO_3^- observed in the seepage water samples. In the selection of the nine variables from among all the observed variables, those with large gaps during the entire observation period, between 1999 and 2010, were excluded, and there were 100 observations for each variable. The data were not required to be normally distributed because PCA is based entirely on an eigenvalue analysis of a correlation or covariance matrix. In this study, the correlation matrix was used in the PCA, as the values for each variable varied by several orders of magnitude.

The stable isotopes (^{18}O and ^{2}H) of water were analyzed in this study to obtain a better understanding of both the interactions between the seepage water and seawater, and the origin of the seepage water salinity. Comparing the oxygen and hydrogen isotope data of the SW with the local meteoric water line (LMWL) could provide information as to whether the samples mainly come from precipitation or not. It was considered that a sample with considerable deviation from the LMWL must have been affected by sources other than precipitation.

Finally, a quantitative analysis for estimating the mixing ratio of seawater in the seepage water was also carried out based on both the Cl^-–Br^- and the Cl^-–$\delta^{18}O$ mixing

ratio. One simple and common method that can be used when quantifying the seawater mixing ratio is to use the Cl^- concentration of seawater and groundwater as two end members and then to calculate the ratio of seawater in a sample of interest (KNOC, 2010). We used both Cl^- and Br^- concentrations when estimating the seawater mixing ratio so as not to overestimate the mixing ratio. From the point where the water samples were located on Cl^-–Br^- and Cl^-–$\delta^{18}O$ plots, an approximate mixing ratio of each sample was analyzed.

4.4 Results

4.4.1 Na^+, Cl^- and EC

The data monitored since 1999 showed that the SW demonstrated distinguishing features, specifically as regards the EC, Na^+, and Cl^-, while most of the water types (IW, MW, WT, and GW) showed chemical characteristics similar to each other. Figure 4.4 shows the ranges of Na^+ and Cl^- concentrations observed in SW and in the other types.

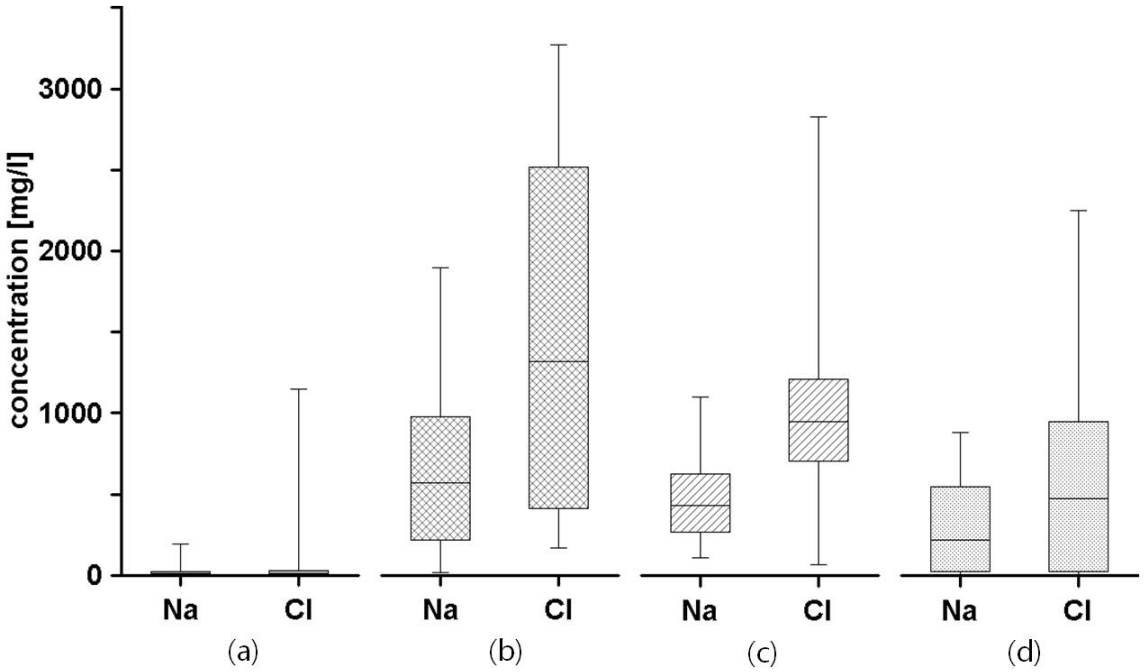

Figure 4.4 Box plot of Na^+ and Cl^- concentrations of (a) IW, MW, WT, and GW, (b) SW of the 1st base, (c) SW of the 2nd base and (d) SW of the 3rd base. Data for IW, MW, WT, GW and SW of the 1st and the 2nd bases are from 1999 to 2010, and for SW of the 3rd base are from 2008 to 2010.

The interquartile range of the Na^+ and Cl^- concentrations from the seepage water are up to two orders of magnitude greater in comparison to that of the other water samples, with values that are rarely observed in freshwater (i.e., 1–250 mg l^{-1} Cl^- according to U.S. drinking water regulations).

The results of the Na^+, Cl^-, and EC observations for the GW samples are shown on the maps in Figure 4.3. It is expected, in general, that the values of Na^+, Cl^-, and EC will increase with the proximity to the sea if seawater intrudes into the cavern area. In the study site, however, no significant relation was noted between the values of Na^+, Cl^-, and EC in groundwater and the distance to the sea from their observation points. Interestingly, high Na^+ and Cl^- concentrations and EC values were observed at groundwater wells located along the major fracture zone, F1-1, which divides the 2nd and the 3rd storage bases (Figure 4.3). For groundwater wells near the F1-1 fracture zone, the mean concentration of Na^+, Cl^-, and EC values were 81.0 mg l^{-1}, 197.3 mg l^{-1}, and 935.5 μS cm^{-1}, respectively, while they were 18.1 mg l^{-1}, 29.5 mg l^{-1}, and 278.9 μS cm^{-1} for the other wells of the 2nd and the 3rd storage bases.

At the seawater barrier wells, the observed EC values were only in the range of 100–300 μS cm^{-1} except at the bottom, which is hardly considered as a sign of seawater intrusion (Figure 4.5). Na^+ and Cl^- concentrations detected at those wells showed similar

value to fresh water, ranging from 10 to 60 mg l^{-1} (Table 4.1).

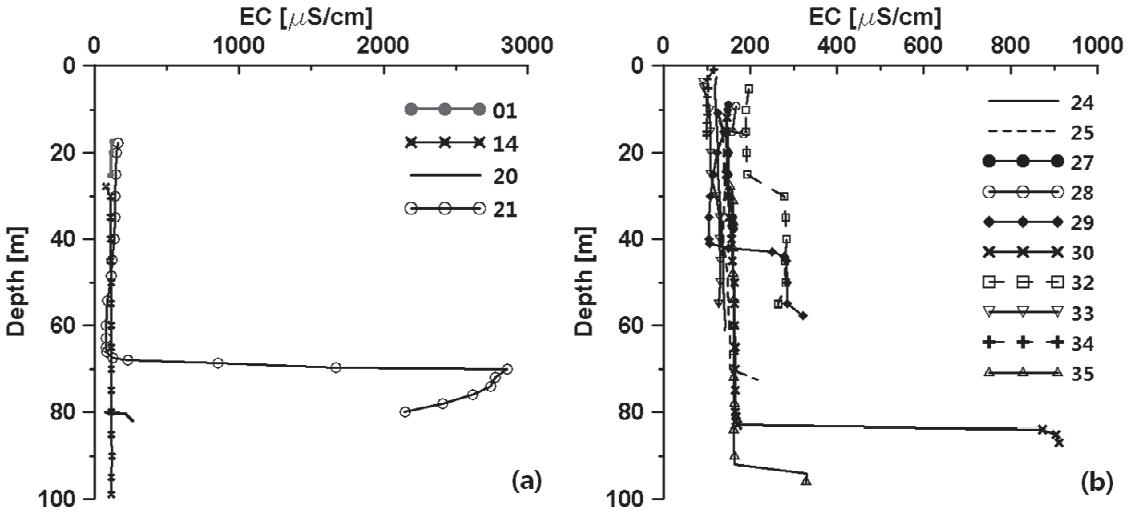

Figure 4.5 EC profile by depth measured at the seawater intrusion barrier wells at (a) the 1st and (b) the 2nd storage bases. Numbers indicate the name of each well as shown in Figures 4.2b and 4.2c.

Table 4.1 Na^+ and Cl^- concentrations measured at seawater intrusion barrier wells

Well number	Depth [m]	Na^+ [mg l^{-1}]	Cl^- [mg l^{-1}]
14	50	9.84	8.08
20	80	4.03	4.08
21	45	15.54	11.16
	75	14.34	10.40
24	40	10.97	7.69
25	72	11.05	7.65
27	35	1.53	8.32
29	50	22.99	8.91
30	50	17.33	11.64
	80	15.11	10.76
32	40	53.55	51.95
33	45	21.96	8.94
35	90	21.80	8.86

4.4.2 Cl^-/Br^- ratio

The Cl^-/Br^- ratio of all water samples near the caverns are plotted against the Cl^- concentration in Figure 4.6. The ranges of the Cl^- concentration and the Cl^-/Br^- ratio for different chloride sources are given in Table 2 based on Alcalá and Custodio (2008).

According to Table 4.2, none of the water samples in our study had a Cl^- concentration within the range of seawater intrusion (Figure 4.6). SW samples showed a slightly lower Cl^- concentration than seawater while displaying a wide range of Cl^-/Br^- ratios.

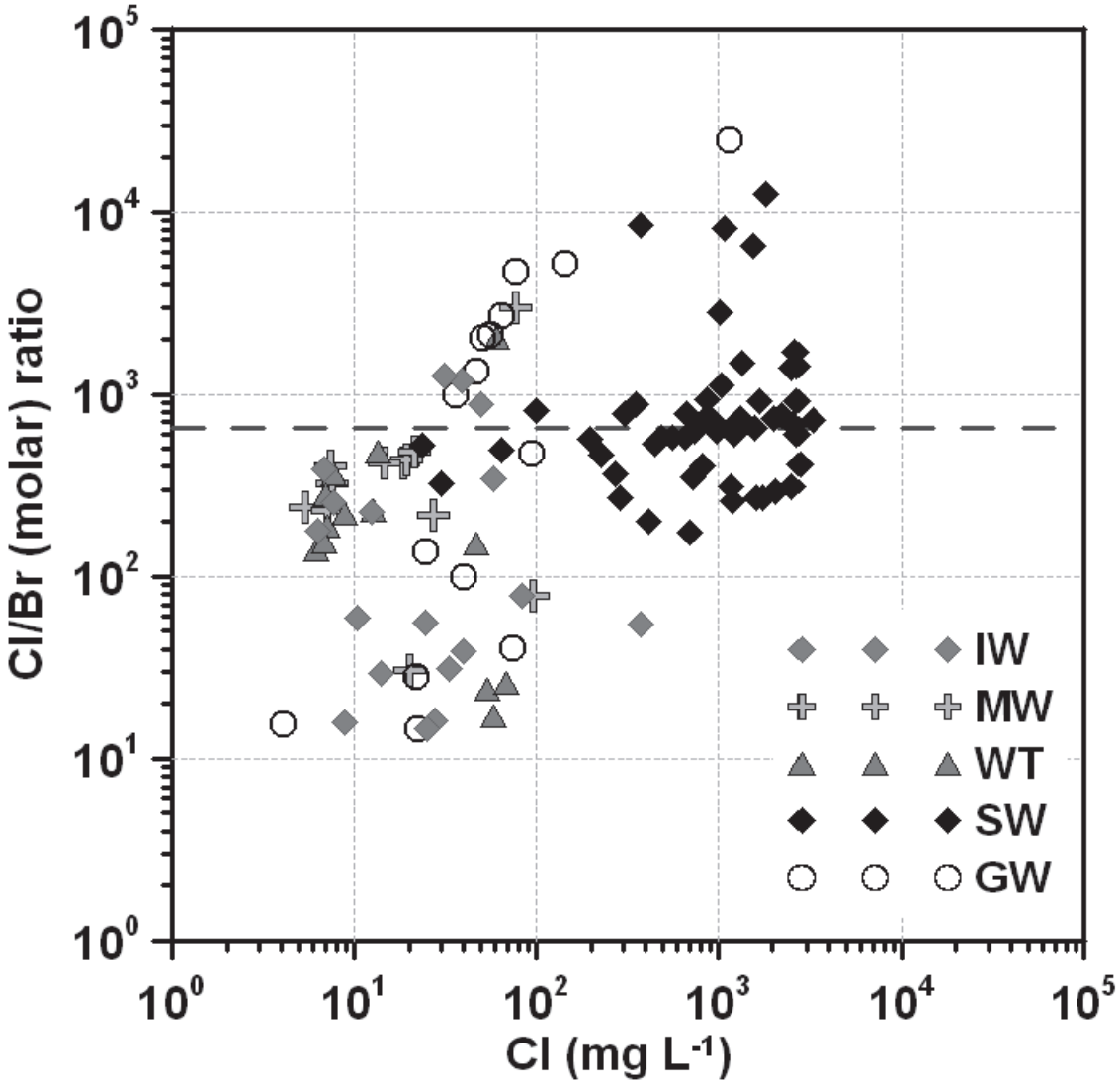

Figure 4.6 Cl^-/Br^- ratios of different type of water samples from Yeosu storage complex.

Table 4.2 Cl^- concentration and Cl^-/Br^- ratios for different types of salinity*

Cl^- (mg l^{-1})	Cl^-/Br^- (molar ratio)	Types of salinity
10–100	200–1300	Recharge waters
300–1100	200–1400	Agricultural pollution, Urban waste water
4000–20000	610–680	Seawater intrusion
19000–20000	655 ± 4	Seawater

* based on Alcalá and Custodio (2008)

4.4.3 Principal component analysis

A statistical overview of the hydrogeochemical data of the variables used in PCA is presented in Table 4.3. Each variable in Table 4.3 was distributed log-normally. The high standard deviation indicates that the temporal and spatial variations are large, which may be caused by the mixing of different sources. PCA results show that the first three principal components accounted for 83.4% of the total variance of the original variables (Figure 4.7). PCs accounting for more than 70% of the variance are considered to be sufficient to represent the information of the original variables (SAS institute Inc., 2009). The first principal component (PC 1), which contributes 52.7% of the total variance, has high loadings for Na^{+}, Ca^{2+}, Mg^{2+}, and Cl^{-}. The second principal component (PC 2), which contributes 16.9% of the total variance, has high loadings for K^{+}, Si, and SO_4^{2-}.

Table 4.3 Statistical data of the variables for PCA

	Mean	**SD***
pH	7.8	1.3
Na^+	218.3	308.6
K^+	13.6	16.3
Ca^{2+}	82.8	108.3
Mg^{2+}	19.2	31.0
Si	8.3	4.8
Cl^-	505.4	760.4
SO_4^{2-}	46.0	86.0
HCO_3^-	59.2	61.4

*SD: Standard deviation

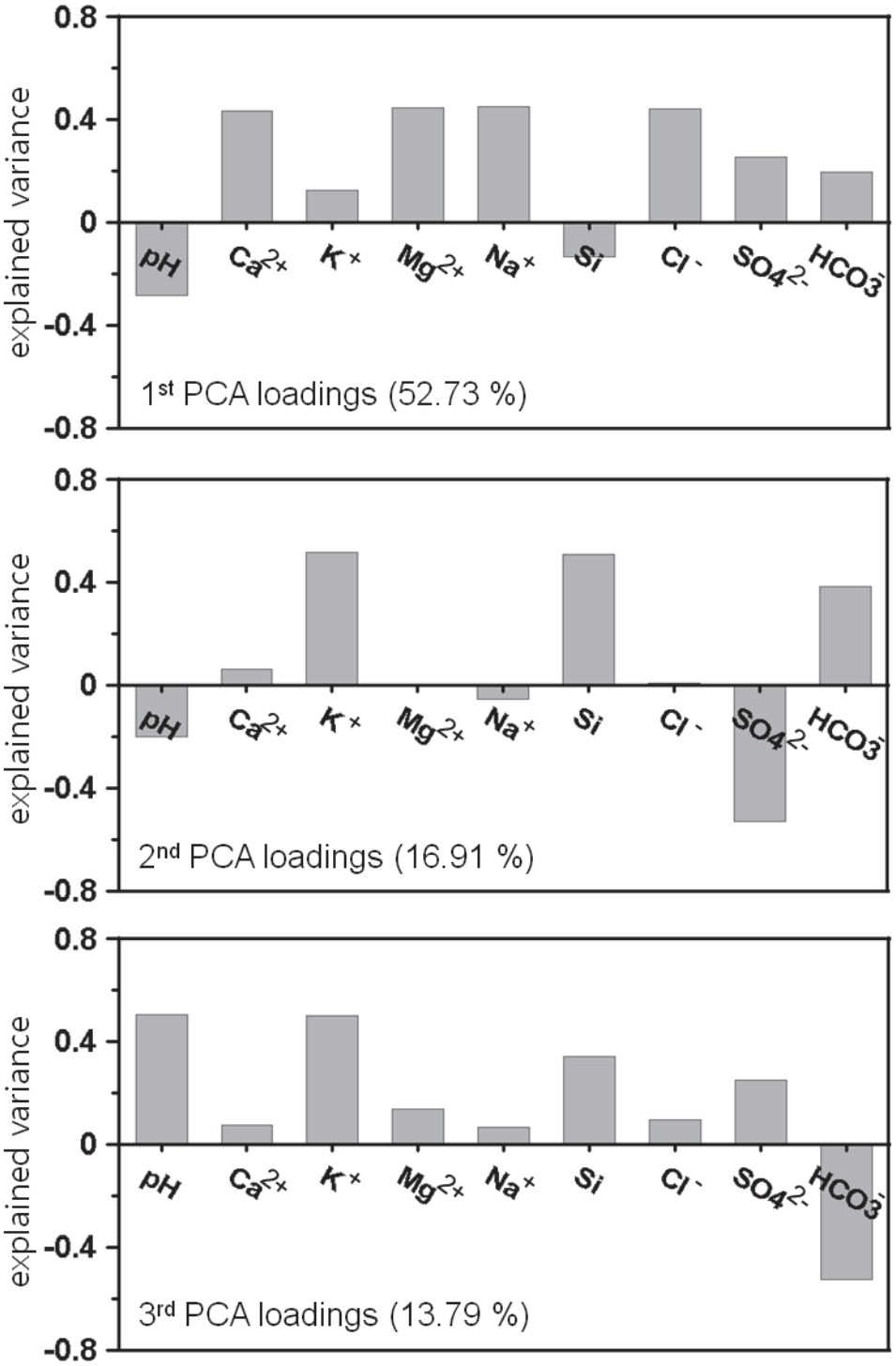

Figure 4.7 PCA loadings for the first three components of the seepage water during the observation period between 1999 and 2010.

In Figure 4.8, the seepage water of each cavern is plotted for PC 1 and PC 2. The influence of seawater mixing and the dissolution of cement materials are plotted in a positive direction on the PC 1 axis, whereas the seepage water affected by the reaction of local bedrock minerals is plotted in a positive direction on the PC 2 axis. The 1st and the 2nd storage bases displayed mostly positive values for PC 1 while the 3rd base showed a wide range of PC 1 values.

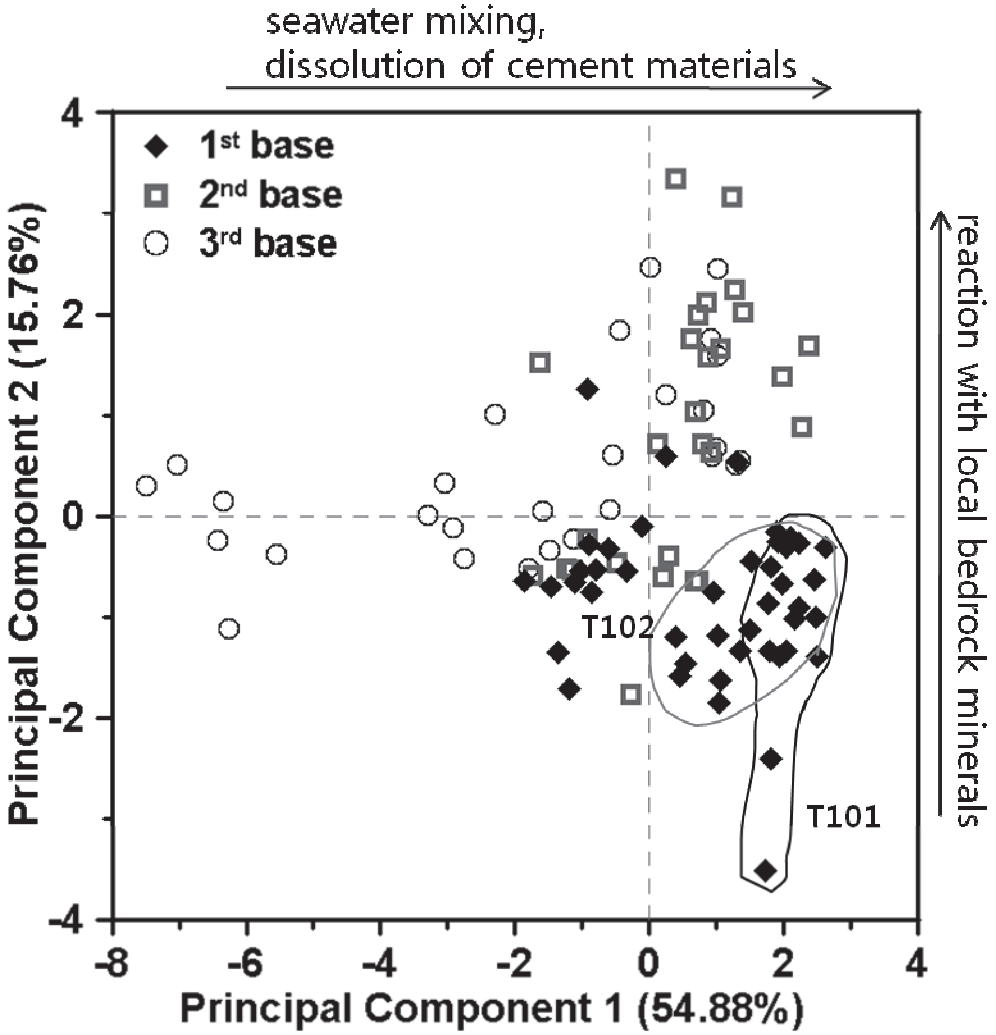

Figure 4.8 Plot of PC1 versus PC2 as the result of PCA of seepage water for 9 variables including pH, Ca^{2+}, K^{+}, Mg^{2+}, Na^{+}, Si, Cl^{-}, SO_4^{2-}, HCO_3^{-}. Those from the T101 and T102 caverns are bounded with solid line.

4.4.4 Stable isotope analysis

The results of oxygen and hydrogen isotope analyses of the seepage water and local groundwater are shown in Figure 4.9. GW sample (Figure 4.9a) results are in good agreement with the LMWL, especially considering that the samples were collected during the summer (Lee and Lee, 1999). The seepage water samples also do not deviate significantly from the LMWL.

The Cl^-–$\delta^{18}O$ relation is also plotted in Figure 4.9b with dashed lines representing the mixing lines of seawater (Cl^- = 19 mg l^{-1}; $\delta^{18}O$ = -0.8‰) and local groundwater (Cl^- = 19 mg l^{-1}; $\delta^{18}O$ = -7.7–-6.5‰). All the seepage water samples are plotted within the range of the groundwater to seawater end members.

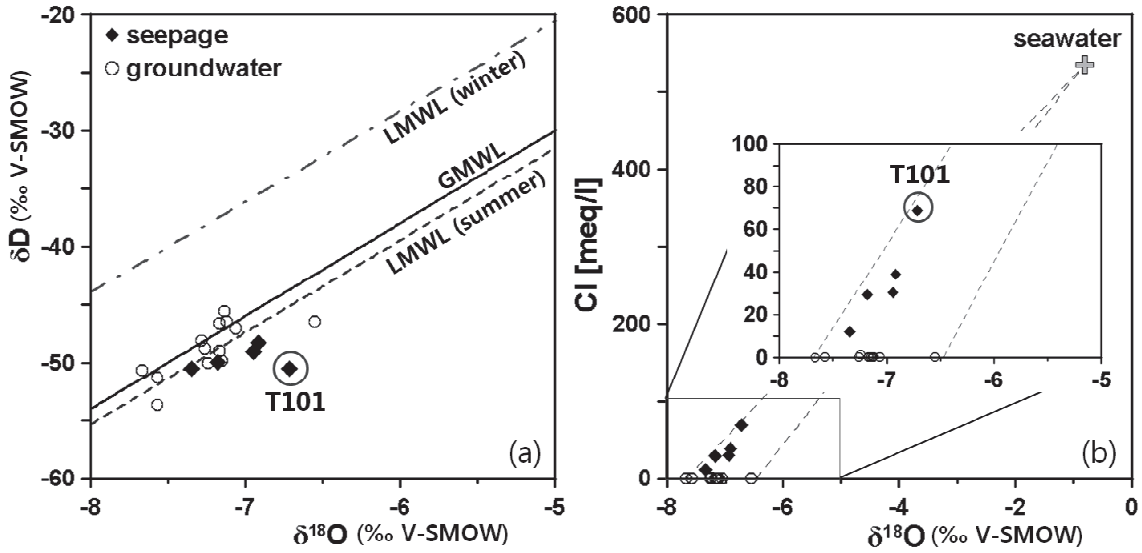

Figure 4.9 Plots of (a) δD versus $\delta^{18}O$ and (b) Cl^- concentration versus $\delta^{18}O$ for seepage and groundwater. The Global Meteoric Water Line (GMWL) is from Craig (1961) and Local Meteoric Water Line (LMWL) is from Lee and Lee (1999).

4.4.5 Cl^--Br^- and Cl^--$\delta^{18}O$ ratio

Figure 4.10 is a bivariate plot of the Cl^-–Br^- mixing ratio using seawater (Cl^- = 19,000 mg l^{-1}; Br^- = 65 mg l^{-1}) and local groundwater (Cl^- = 19 mg l^{-1}; Br^- = 1 mg l^{-1}) as the two end members. The solid line in the plot shows the conservative mixing line of the two end members. Assuming that the Cl^- and Br^- in the samples originate only from seawater and local groundwater, a point represented by the Cl^-–Br^- mixing ratio of each sample should lie on the mixing line. While some points do not agree with the mixing line, many of the points show a tendency similar to that of the mixing line. The highest mixing ratio on the line was estimated to be about 14% for the seepage water from T101. The maximum mixing ratio estimated using only Cl^- was 17.9%, while that using only Br^- was 27.1%, which are overestimations of the ratio compared to the value when both Cl^- and Br^- ions are used.

The Cl^-–$\delta^{18}O$ relation is also plotted in Figure 4.9b with the dashed lines representing the mixing lines of seawater (Cl^- = 19 mg l^{-1}; $\delta^{18}O$ = -0.8‰) and local groundwater (Cl^- = 19 mg l^{-1}; $\delta^{18}O$ = -7.7–-6.5‰). All of the seepage water samples are plotted within the range of the groundwater to seawater end members.

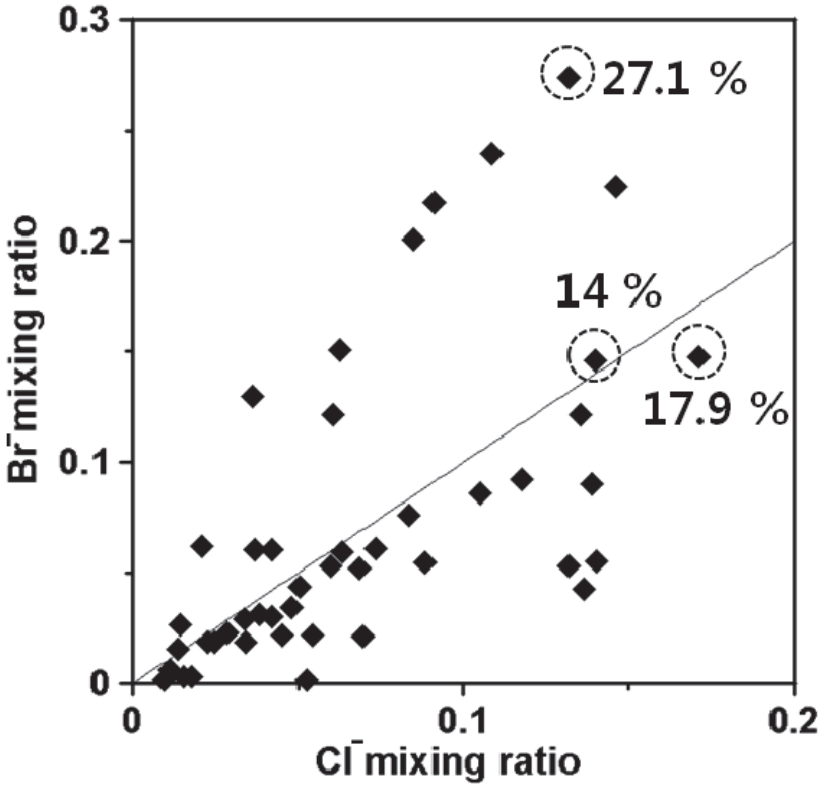

Figure 4.10 Bivariate plot of mixing ratios of seawater and the seepage water samples. The solid line in the plots represents the mixing line of seawater (Cl^- = 19,000 mg l^{-1}; Br^- = 65 mg l^{-1}) and local groundwater (Cl^- = 19 mg l^{-1}; Br^- = 1 mg l^{-1}).

4.5 Discussion

4.5.1 Chances of seawater intrusion

The results of Na^+, Cl^-, and EC observation (Figure 4.3) suggest that the F1-1 fracture zone may provide a preferential pathway for seawater to influence inland freshwater near the 2nd and the 3rd bases. The role of the F1-1 fracture zone in seawater mixing with groundwater at this site was also evaluated through a numerical simulation (KNOC, 2011; Lee et al., 2012). The simulation also showed F1-1 as a preferential pathway of seawater intrusion. Similar spatial variations in the chemical composition of groundwater and in the seawater intrusion through fractures were reported in other studies (Allen et al., 2002; Subba Rao et al., 2005).

Meanwhile, seawater intrusion from the coastline is doubtful when considering the observation results at the seawater intrusion barrier wells and hydraulic head distribution of the area. The Na^+ and Cl^- concentrations at the barrier wells (Table 4.1) along with IW, MW, WT, and GW (Figure 4.4a) do not suggest any intrusion of seawater through this pathway. Thus, the dramatic increase in EC at the bottom of some wells (Figure 4.5) is suspected to be an outcome of biological or abiological corrosion rather than seawater intrusion. Hydraulic head at the cavern is lower than the surrounding area, which makes groundwater flow from the hilly area through the cavern,

then to the coast. Thus, seawater intrusion toward the front of the cavern at the cavern depth has little possibility. Therefore, the abnormally high Cl^- concentration observed in the seepage water, specifically at the 1st base, is suspected to have originated not from the coastal side but possibly from seawater inflow through the bottom of the caverns (KNOC, 2011; Lee et al., 2012).

With the overall results of Na^+, Cl^-, and EC observations in consideration of their observation location in geological setting, a detailed insight about the seawater intrusion pathway is deduced.

4.5.2 Origin of the salinity

The Cl^-/Br^- ratio result (Figure 4.6) implies that there are sources other than seawater which caused the high Cl^- content in SW. The wide range of the Cl^-/Br^- ratio suggests the possibility of influence of brines dispersed in the stored oil. However, according to KNOC, the amount of brine in the oil of Yeosu base is only 0.05% of total volume of the stored oil. Since the purpose of oil storage in Yeosu base is to stockpile, there is rarely shipment or arrival of oil, and this limit the supply of brine to the cavern. In addition, freshwater injection through IW of water curtain system and extraction of the seepage water must have diluted the brine, possibly existed in the cavern at the early

stage. Based on this fact, it can be inferred that the brine in the stored oil would not have significant influence on the salinity in seepage water. Additional understanding of the sources was deduced from the PCA result (Figure 4.7). Regarding PC 1, the high loadings for Na^+, Mg^{2+}, and Cl^- were likely associated with the mixing of seawater, and pH and Ca^{2+} level are suspected to be related to the dissolution of encrusted cement materials. The high loadings for K^+ and Si of PC 2 can be explained by hydrochemical interactions between local bedrock minerals.

While each PC contains information about the sources of the salinity of the seepage water, Figure 4.8 shows that there is some spatial variance in the influence of difference sources. The seepage water from T101 and T102 in the 1st base, having the highest PC1 values, appears to be influenced most by the mixing of seawater and cement dissolution. The reactions of bedrock minerals appear to be the most influential on the seepage water of the 2nd storage base, which had higher PC 2 values, while the 1st storage base displayed lower values. The wide range of PC 1 values shown by the seepage water from the 3rd storage base is supposed to have resulted owing to the F1-1 fracture zone developed close to the storage base, as shown in Figure 4.2a. The F1-1 fracture zone, which appears to act as a pathway for seawater to mix with the seepage water of the 3rd base, seems to increase the complexity of the hydrogeological

conditions, causing the PC 1 values for the 3rd storage base to vary widely.

The analysis of the Cl^-/Br^- ratios and the PCA results show that a certain amount of seawater is mixed into the seepage water. The pattern presented by PCA for each cavern also shows that the geological features, including the F1-1 fracture zone, in the storage base area can increase the heterogeneity under hydrogeological and hydrochemical conditions of the site.

The results from the isotope analysis also support the preceding analysis. T101 SW, which is influenced by the seawater mixing and cement dissolution according to the PCA, showed the greatest degree of deviation from the LMWL (Figure 4.9a). The Cl^-–$\delta^{18}O$ relation (Figure 4.9b) suggests that seawater and local groundwater make major contributions to the content of the seepage water. The highest Cl^- concentration was also observed at T101 SW. The influence of seawater on T101 seepage water implied from the isotope analysis may not be apparent but it is more than negligible as shown in chloride concentration of Figure 4.9(b).

4.5.3 Extent of seawater mixing

Although seawater may not be the only source of the high ion concentration in the seepage water, it is still the main contributor to the chemical characteristics of the

seepage water. Thus, we evaluated the seawater mixing ratio in the seepage water. This implies that the seepage water quality was influenced by seawater and by other sources.

Using the Cl^-–Br^- mixing ratio and the Cl^-–$\delta^{18}O$ relation, the extent of seawater mixing in the seepage water was estimated (Figure 4.10). Although the basis of the estimation is rather rough, assuming only two end members (seawater and local groundwater) as the origins of Cl^-, Br^-, and $\delta^{18}O$, they showed consistent results, estimating 14% of seawater in T101 seepage water. The maximum estimate of the mixing ratio in each cavern using the Cl^-–Br^- mixing ratio is given in Table 4.4. Based on these results, we suggest that seawater is being mixed with the cavern seepage water in amounts up to 14% from the bottom of the cavern at the 1st and 2nd base, as well as through the major fracture zone at the 3rd base.

Table 4.4 The maximum estimate of mixing ratio in seepage water (SW) at each cavern using the Cl^-–Br^- mixing ratio

cavern	**mixing ratio**	**cavern**	**mixing ratio**
T101	14%	T411	~1%
T102	8%	T421	~1%
T103	~1%	T431	2%
T201	2%	T441	6%
T202	6%	T451	2%
		T461	3%

4.6 Conclusion

This work investigates the origins and inflow routes of the salinity of the seepage water and assesses the extent of the seawater intrusion by using hydrogeochemical analysis integrated with hydrogeological observations. While GW readings display high concentrations of Na^+ and Cl^- only near the F1-1 location, the influence of seawater on SW is revealed by Cl^-/Br^- ratio analysis, PCA, and isotope analysis. In the quantification of the mixing ratio of seawater in the seepage water, an integrated approach involving the use of Cl^-–Br^- mixing ratio and isotope analysis was used. Integrating the results lead to the conclusion that seawater is mixed into the seepage water through the lower part of the bedrock under the cavern near the 1st base and through the local fracture zone near the 2nd and the 3rd bases. In addition, the seepage water from each cavern was found to have different chemical characteristics and a different mixing ratio, possibly because of geological heterogeneity of the site. The maximum 14% of seawater mixing ratio was shown at the T101 cavern and relatively low mixing ratios (i.e., 1–8%) in the other caverns. Specifically at the caverns of the 2nd and the 3rd bases, the mixing ratio was less than 6%. A comprehensive understanding of seawater intrusion in this complex environment involving a fractured aquifer and artificial structures is achieved with the integrated investigation.

Concluding Remarks

This study focuses on analyzing groundwater contamination from coupled environmental-anthropogenic sources. Groundwater contamination derived from interaction of human-natural activities needs to be analyzed with multiple methods for better understanding of the contaminated sites.

At an agricultural site where land uses are highly occupied with vegetation activities groundwater showed elevated level of nitrate concentration. This study analyzed relation between the types of land use of the area and nitrate concentration of local groundwater. The probabilistic capture zone derived from a numerical modeling of solute transport is integrated into Tobit regression analysis. The result showed that anthropogenic activities, specifically vegetation, are closely related to the nitrate concentration. The regression model integrated with the probabilistic capture zone presented better results in analyzing the land use-groundwater quality relation than using normal regression method.

Detection of leachate transport from a livestock burial was studied with solute transport modeling and the measure of the electrical resistivity of subsurface. Since the site of this study was very limited in available monitoring wells, the measure of

electrical resistivity was an alternative method to calibrate transport simulation model. For quantitative assessment of model calibration, the raster image of electrical resistivity of a section was compared with that of solute distribution contour of the simulation. The results showed that this method could be a efficient substitute of well monitoring data for field site with limited access.

The study of salinity invasion near coastal area with underground storage facility was approached with hydrogeochemical analysis integrated with thorough consideration of hydrogeological observation. Ion ratio analysis, PCA, and isotope analysis were performed. The results of each analysis were not appeared to be in good accordance however, close investigation of the results in the context of hydrogeology led to the conclusion that there was a preferential pathway of seawater intrusion and there were local differences in intensity of seawater mixing.

All the above mentioned study results showed that the selection and integration of reasonable methods in analysis of groundwater contamination from coupled environmental-anthropogenic sources can improve our understanding about the source of contaminants and thus enable us to plan sustainable groundwater management.

References

Alcalá, F.J., and E. Custodio. 2008. Using the Cl/Br ratio as a tracer to identify the origin of salinity in aquifers in Spain and Portugal. J. Hydrol. 359: 189-207.

Allen, D.M., D.G. Abbey, D.C. Mackie, R.D. Luzitano, and M. Cleary. 2002. Investigation of potential saltwater intrusion pathways in a fractured aquifer using an integrated geophysical, geological and geochemical approach. J. Environ. Eng. Geophys. 7(1): 19-36.

Aller, L., T. Bennett, J.H. Lehr, R.J. Petty, and G. Hackett. 1987. DRASTIC: a standardized system for evaluating groundwater pollution potential using hydrogeological setting. EPA/600/2-87/035, Robert S. Kerr Environmental Research Laboratory, US Environmental Protection Agency, Rep, Oklahoma.

Alley, W.M., R.W. Healy, J.W. LaBaugh, and T.E. Reilly. 2002. Flow and Storage in Groundwater Systems. Science. 296:1985-1990.

Antonakos, A.K., and N.J. Lambrakis. 2007. Development and testing of three hybrid methods for the assessment of aquifer vulnerability to nitrates, based on the drastic model, an example from NE Korinthia, Greece. J. Hydrol. 333:288-304.

Barringer, T.H., D. Dunn, W.A. Battaglin, and E.F. Vowinkel. 1990. Problems and

methods involved in relating land use to ground-water quality. Water Resour. Bull. 26(1): 1-9.

Binley, A., C. Giorgio, M. Roy, and W. Peter. 2002a. Vadose zone flow model parameterization using cross-borehole radar and resistivity imaging, J. of Hydrol. 267: 147-159.

Chang, H.W., and K.-K. Lee. 1998. Study on the effect of industrial waste disposal on the facilities of underground LPG storage caverns. Research Institute for Basic Sciences, Seoul Natl. Univ., Seoul, Korea.

Choi, W.-J., G.-H. Han, S.-M. Lee, G.-T. Lee, K.-S. Yoon, S.-M. Choi, and H.-M. Ro. 2007. Impact of land-use types on nitrate concentration and $\delta^{15}N$ in unconfined groundwater in rural areas of Korea. Agriculture, Ecosystems & Environment 120(2-4): 259-268.

Cornaton, F. 2003. Deterministic models of groundwater age, life expectancy and transit time distributions in advective-dispersive systems. Ph.D. diss. Center of Hydrogeology, Institute of Geology, University of Neuchtel. Neuchtel, Switzerland.

Craig, H. 1961. Isotopic variation in meteoric waters. Science 33: 1702-1703.

Daily, W., A. Ramirez, A. Binley, and D. LaBrecque. 2004. Remote monitoring of leaks in storage tanks using electrical resistance tomography: application at the Hanford

Site. Journal of Environment and Engineering Geophysics 9:11-24.

Dallal, G.E. 2007. The Little Handbook of Statistical Practice. Available at http://www.StatisticalPractice.com (verified Oct. 2008). Boston, MA.

Davis, S.N., J. Fabryka-Martin, and L.E. Wolfsberg. 2004. Variations of bromide in potable ground water in the United States. Ground Water 42(6): 902-909.

Davis, S.N., D.O. Whittemore, and J. Fabryka-Martin. 1998. Uses of chloride/bromide ratios in studies of potable water. Ground Water 36(2): 338-350.

Demirel, Z., 2004. The history and evaluation of saltwater intrusion into a coastal aquifer in Mersin, Turkey. J. Environ. Management 70(3): 275-282.

Diersh, H.J.G. 2002. FEFLOW-Physical basis of modelling. WASY Institute for Water Resource Planning and Systems Research Ltd. Berlin, Germany

Doerfliger, N., P.Y. Jeannin, and F. Zwahlen. 1999. Water vulnerability assessment in karst environments: a new method of defining protection areas using a multi-attribute approach and GIS tools (EPIK method). Environ. Geol. 39(2):165-176.

Eckhardt, D.A.V., and P.E. Stackelberg. 1995. Relation of ground-water quality to land use on Long Island, New York. Ground Water. 33(6):1019-1033.

Epstein, S., and T.K. Mayeda. 1953. Variation of ^{18}O content of waters from natural sources. Geochim. Cosmochim. Acta 4: 213-224.

Frind, E.O., J.W. Molson, and D.L. Rudolph. 2006. Well vulnerability: a quantitative

approach for source water protection. Ground Water. 44(5):732-742.

Gardner, K.K., and R.M. Vogel. 2005. Predicting ground water nitrate concentration from land use. Ground Water. 43(3):343-352.

Gasperikova, E., S. Hubbard, D.B. Watson, G.S. Baker, J.E. Peterson, M.B. Kowalsky, M. Smith, and S. Brooks. 2012. Long-term electrical resistivity monitoring of recharge-induced contaminant plume behavior. J. of Contaminant Hydrol., 142-143:33-49.

Geostock. 1992. Ulsan LPG storage caverns Yukong gas hydrogeological monitoring. Geostock, Paris.

Gurdak, J.J., and S.L. Qi. 2006. Vulnerability of recently recharged ground water in the High Plains aquifer to nitrate contamination. U.S. Geological Survey Scientific Investigations Report 2006-5050., 39p.

Hesser, F.B., U. Franko, and M.Rode. 2010. Spatially distributed lateral nitrate transport at the catchmen scale. J. Environ. Qual. 39:193-203.

Hubbard, S.S., J.E. Peterson, E.L. Majer, P.T. Zawislanski, K.H. Williams, J. Roberts, and F. Wobber. 1997. Estimation of permeable pathways and water content using tomographic radar data. Leading Edge, 1623–1628.

Kaown, D., Y. Hyun, G.O. Bae, and K.K. Lee. 2007. Factors affecting the spatial

pattern of nitrate contamination in shallow groundwater. J. Environ. Qual. 36:1479-1487.

Kaown, D., K.K. Lee, and D.C. Koh. 2009. Effects of groundwater residence time and recharge rate on nitrate contamination deduced from $\delta^{18}O$, δD, $^{3}H/^{3}He$ and CFCs in a small agricultural area in Chuncheon, Korea. J. Hydrol. 336:101-111.

Kemna, A., B. Kulessa, and H. Vereecken. 2002. Imaging and characterisation of subsurface solute transport using electrical resistivity tomography (ERT) and equivalent transport models. J. of Hydrol. 267(3-4): 125-146.

KIGAM. 2012. Microbial characterization and transport modelling of leachate from animal carcass disposal. Final report. Korea Institute of Geoscience and Mineral Resources, Korea (in Korean)

Kim, J.H., R.H. Kim, J. Lee, and H.W. Chang. 2003. Hydrogeochemical characterization of major factors affecting the quality of shallow groundwater in a coastal area, Kimje in South Korea. Environ. Geol. 44(4): 478-489.

Kim, Y.J., and S. Hamm. 1999. Assessment of the potential for ground water contamination using the DRASTIC/ EGIS technique, Cheongju area, South Korea. Hydrogeol. J. 7(2):227-235.

Kim, T., K.-K. Lee, K.S. Ko, and H.W. Chang. 2000. Groundwater flow system inferred

from hydraulic stresses and heads at an underground LPG storage cavern site. J. Hydrol. 236: 165-184.

KNOC, 2010. R&DB collaborated research on maximizing period of depreciation of underground storage cavern, Final report. Korea Natl. Oil Co., Korea (in Korean).

KNOC, 2011. Research on water quality and geochemical problems of underground storage cavern complex, Final report. Korea Natl. Oil Co., Korea (in Korean).

Koukadaki, M. A., G. P. Karatzas, M. P. Papadopoulou, and A.Vafidis. 2007. Identification of the saline zone in a coastal aquifer using electricaa tomography data and simulation. Water Resource Manage. 21:1881-1898.

Kowalsky, M.B., E. Gasperikova, S. Finsterle, D. Watson, G. Baker, and S.S. Hubbard. 2011. Coupled modeling of hydrogeochemical and electrical resistivity data for exploring the impact of recharge on subsurface contamination. Water Resources Research, 47: W02509

Kroll, C.N., and J.R. Stedinger. 1999. Development of regional regression relationships with censored data. Water Resour. Res. 35(3):775-784.

Lambrakis, N., A. Antonakos, and G. Panagopoulos. 2004. The use of multicomponent statistical analysis in hygrogeological environmental research. Water Research. 38:1862-1872.

Lee, E., 2012. Quantitative assessment of groundwater discharges and inflow fluxes due to dynamic interactions between groundwater and surface water. Ph.D. thesis, School of Earth and Environmental Sciences, Seoul National University, Seoul, Korea.

Lee, J., J.-H. Kim, H.-M. Kim, and H.-W. Chang. 2007. Statistical approach to determine the salinized ground water flow path and hydro geo chemical features around the underground LPG cavern, Korea. Hydrol. Process. 21: 3615-3626.

Lee, J., R.-H. Kim, and H.-W. Chang. 2003. Interaction between groundwater quality and hydraulic head in an area around an underground LPG storage cavern, Korea. Environ. Geol. 43: 901-912.

Lee, J., K.-S. Ko, J.-M. Kim, and H.-W. Chang. 2008. Multivariate statistical analysis of underground gas storage caverns on groundwater chemistry in Korea. Hydrol. Process. 22: 3410-3417.

Lee, J.Y., J.Y. Cheon, K.K. Lee, S.Y. Lee, and M.H. Lee. 2001. Statistical evaluation of geochemical parameter distribution in a groundwater system contaminated with petroleum hydrocarbon. Journal of Environmental Quality 30: 1548-1563.

Lee, K.S., and C.B. Lee. 1999. Oxygen and hydrogen isotopic composition of precipitation and river waters in South Korea. J. Geol. Society of Korea 35(1): 73-

84 (in Korean).

Li, Jing, and B.-L. Lu. 2009. An adaptive image Euclidean distance, Pattern Recognition. 42: 349-357.

Lim, J.-W., G.O. Bae, and K.K. Lee. 2009. Groundwater vulnerability assessment by determining maximum contaminant loading limit in the vicinity of pumping wells. Geosci. J. 13(1):79-85.

Lim. J.-W., E. Lee, H. S. Moon, and K.-K. Lee. 2013. Integrated investigation of seawater intrusion around oil storage caverns in a coastal fractured aquifer using hydrogeochemical and isotopic data. J. Hydrol. 486:202-210.

Liu, S., J. Lu, D.W. Kolpin, and W.Q. Meeker. 1997. Analysis of environmental data with censored observations. Environ. Sci. Technol. 31(12):3358-3362.

McLay, C.D.A., R. Dragden, G. Sparling, and N. Selvarajah. 2001. Predicting groundwater nitrate concentrations in a region of mixed agricultural land use: a comparison of three approaches. Environ. Pollut. 115:191-204.

MOLIT and K-water. 2011. Fundamental investigation of groundwater of Icheon. Final report. Ministry of Land, Transport and Maritime Affairs. Korea Water Resources Corporation, Korea (in Korean).

Monego, M., G. Cassiani, R. Deiana, M. Putti, G. Passadore, and L. Altissimo. 2010.

Tracer test in a shallow heterogeneous aquifer monitored via time-lapse surface ERT. Geophysics 75(4): WA61-WA73.

Morell, I., E. Giménez, and M.V. Esteller. 1996. Application of principal components analysis to the study of salinization on the Castellon Plain (Spain). Sci. Total Environ. 177: 161-171.

Morrison, J., T. Brockwel, T. Merren, F. Fourel, and A.M. Phillips. 2001. On-line high precision stable hydrogen isotopic analyses on nanoliter water samples. Anal. Chem. 73: 3570-3575.

Moutsopoulos, K.N., A. Gemitzi, and V.A. Tsihrintzis. 2009. Delineation of groundwater protection zones by the backward tracking method: Theoretical background and GIS-based stochastic analysis. Environ. Geol. 53:1081-1090.

Neupauer, R.M., and J.L. Wilson. 1999. Adjoining method for obtaining backward-in-time location and travel time probabilities of a conservative groundwater contaminant. Water Resour. Res. 35(11):3389-3398.

Neupauer, R.M., and J.L. Wilson. 2001. Adjoint-derived location and travel time probabilities for a multidimensional groundwater system. Water Resour. Res. 37(6):1657-1668.

Nolan, B.T. 2001. Relating nitrogen sources and aquifer susceptibility to nitrate in

shallow ground waters of the United States. Ground Water. 39:290-299.

Palmer, R.C., and M.A. Lewis. 1998. Assessment of groundwater vulnerability in England and Wales. P.191-198. *In* N.S. Robins (ed.) Groundwater Pollution, Aquifer Recharge and Vulnerability. Geological Society. Special Publication, 130. London.

Panagopoulos, G.P., A.K. Antonakos, and N.J. Lambrakis. 2006. Optimization of the DRASTIC method for groundwater vulnerability assessment via the use of simple statistical methods and GIS. Hydrogeol. J. 14:894-911.

Panno, S.V., K.C. Hackley, H.H. Hwang, S.E. Greenberg, I.G. Krapac, S. Landsberger, D.J. O'kelly. 2006. Characterization and identification of Na-Cl sources in ground water. Ground Water 44 (2): 176-187.

Perri, M.T., G. Cassiani, I. Gervasio, R. Deiana, and A. Binley. 2012. A saline tracer test monitored via both surface and cross-borehole electrical resistivity tomography: Comparison of time-lapse results, Journal of Applied Geophysics, 79: 6-16.

Ramirez, A., W. Daily, A. Binley, D. LaBrecque and D. Roelant. 1996. Detection of leaks in underground storage tanks using electrical resistance methods. J. Environ. and Eng. Geophysics 1:189-203.

Ramstad, E., and J. Woo. 2011. Foot-and-Mouth disease roils Korean Farms. The Wall

Street Journal. 2011-01-11.

Sánchez-Martos, F., A. Pulido-Bosch, L. Molina-Sánchez, and A. Vallejos-Izquierdo. 2002. Identification of the origin of salinization in groundwater using minor ions (Lower Andarax, Southeast Spain). Sci. Total Environ. 297: 43-58.

SAS Institute. 2003. SAS for Windows, Version 9.1. SAS Inst., Cary, NC.

SAS institute Inc., 2009. SAS for Windows. Version 9.2. SAS Institute Inc., Cary, NC.

Sener, E., S. Sener, and A. Davraz. 2009. Aseessment of aquifer vulnerability based on GIS and DRASTIC methods: A case study of the Senirkent-Uluborlu Basin (Isparta, Turkey). Hydrogeol. J. 17:2023-2035.

Stigter, T.Y., L. Ribeiro, and A.M.M. Carvalho Dill. 2008. Building factorial regression models to explain and predict nitrate concentrations in groundwater under agricultural land. J. Hydrol. 357:42-56.

Stumm, W., and J.J. Morgan. 1996. Aquatic Chemistry. Wiley, New York.

Subba Rao, N., I. Saroja Nirmala, and K. Suryanarayana. 2005. Groundwater quality in a coastal area: a case study from Andhra Pradesh, India. Environ. Geol. 48: 543-550.

Tesoriero, A.J., and F.D. Voss. 1997. Predicting the probability of elevated nitrate concentrations in the Puget Sound basin: Implication for aquifer susceptibility and vulnerability. Ground Water. 35(6):1029-1039.

Therrien, R., R.G. McLaren, E.A. Sudicky, and S.M. Panday. 2005. HydroGeoSphere: A Three-dimensional Numerical Model Describing Fully-integrated Subsurface and Surface Flow and Solute Transport. Université Laval, and University of Waterloo. Canada.

Tobin, J. 1958. Estimation of relationships for limited dependent variables, Econometrica 26(1):24-36.

Tosco, T., and R. Sethi. 2010. Comparison between backward probability and particle tracking methods for the delineation of well head protection areas. Environ. Fluid Mech. 10:77-90.

Vandenschrick, G., B. van Wesemael, E. Frot, A. Pulido-Bosch, L. Molina, M. Stiévenard, and R. Souchez. 2002. Using stable isotope analysis (δD-$\delta^{18}O$) to characterize the regional hydrology of the Sierra de Gador, south east Spain. J. of Hydrol. 256(1-4): 43-55.

van Overmeeran, R.A., J.C. Gehrels, and S.V. Sariowa. 1997. Ground penetrating radar for determining volumetric soil water content: results of comparative measurements at two test sites. J. Hydrol.197: 316–338.

Voss, C.I. 1984. A finite element simulation model for unsaturated-saturated fluid density-dependent ground water flow with energy transport or chemically reactive

single-species solute transport. USGS Water Resource Investigations Report 84-4369. US Geological Survey.

Wald, A. 1945. Sequential tests of statistical hypotheses. Annals of Mathematical Statistics. 16:117-186.

Wang, L., Y. Zhang, and J. Feng. Aug. 2005 On the Euclidean distance of images. IEEE Trans Pattern Analysis and Machine Intelligence. 27(8):1334-9

Wong, C. 2011. South Korea reportedly buries 1.4 million pigs alive to combat foot and mouth disease. The Huffington Post. 2011-01-12.

Yen, S.T., S. Liu, and D.W. Kolpin. 1996. Analysis of nitrate in near-surface aquifer in the midcontinental United States: An application of the inverse hyperbolic sine Tobit model. Water Resour. Res. 32(10):3003-3011.

Yu, J.Y., I.K. Choi, and H.S. Kim. 1994. Geochemical characteristics of the surface water depending on the bedrock type in the Chuncheon area. J. Geol. Soc. Korea 30(3):307-324.

Zheng, C., M.C. Hill, and P.A. Hsieh. 2001. MODFLOW-2000, the U.S. Geological Survey modular ground-water model – User guide to the LMT6 package, the linkage with MT3DMS for multi-species mass transport modeling. Open-file Report 01-82. U.S. Geology Survey.

국문 초록

지하수 오염은 환경적인 요인, 인위적인 요인 등이 결합된 다양한 원인으로 인해서 발생하는 경우가 많다. 따라서 오염 조사 현장의 특성에 부합하는 적절한 방법들을 다양하게 적용해서 지하수 오염을 분석하는 것이 필요하다. 본 연구는 각 현장의 특성에 따라 적용 가능하거나 필요한 오염 분석 방법들을 적절하게 통합하여 지하수 오염을 평가하는 방법을 제시하고 있다. 본 논문의 세 가지 주제는 각각 서로 다른 환경에서 다른 원인에 의한 지하수 오염을 분석하는 것을 다루고 있다.

첫 번째 주제는 농촌지역에서 지하수 오염을 평가하는 내용으로 지하수 내의 용질 이동을 수치모의 하는 방법과 다변량 회귀분석 방법을 통합하여 토지 이용 양상이 지하수 수질에 미치는 영향을 정량화 하는 방법을 제시하고 있다. 이를 위해 용질 이동의 물리적 과정을 반영한 역방향 이동 방정식을 사용하여 확률적 포획권을 설정하였다. 확률적 포획권은 관정 인근에서 오염물질의 유출이 발생할 때 관정에서 양수되는 지하수 수질이 그 영향을 받게 되는 유출 영역과 그 정도를 확률 값으로 나타내어 준다. Tobit 회귀 분석은 종속 회귀 변수들과 독립 변수의 상관관계를 분석하는 방법의 하나로 본 연구에서는 오염물질의 농도를 독립 변수로 하여 다른 요소들이 지하수 농도에 미치는 영향을 살펴보기 위해 사용 되었다. 확률적

포획권과 회귀분석법을 통합한 모델을 통해서 연구 현장인 춘천의 소규모 농업 분지의 관정에서 검출된 질산성 질소의 농도가 인근의 밭, 과수원, 축사 등에 의해 얼마나 영향을 받는지를 알아 보았다.

두 번째 주제는 가축 매몰지에서 발생하는 침출수의 거동에 관한 연구로 매몰지라는 연구 현장의 특성상 관측과 지하수 시료 수집 등에 관한 활동이 자유롭지 못하다는 제약이 있는 조건에서 진행되었다. 지하수 관정을 사용하는 것이 제한적이라는 점을 극복하고 사용할 수 있는 자료를 수집하기 위해서 전기비저항 탐사가 진행되었다. 측정된 전기비저항 값은 연구 현장의 침출수 모델링 결과와 비교하여 모델의 유효성을 검증하는데 사용되었다. 전기비저항 탐사 결과를 보여주는 그림과 침출수 분포를 보여주는 모델링 결과 그림의 유사성을 정량적으로 비교해서 자료가 제한적인 상태에서 만들어진 수치모델을 침출수 거동을 예측하는데 사용할 수 있도록 했다.

마지막 주제는 수리지화학 자료와 안정동위원소를 사용하여 여수 해안가에 위치한 지하 석유 비축 기지의 염화된 삼출수의 특성을 분석, 염분의 기원과 유입 경로를 분석하는 연구이다. 연구 지역은 해안가라는 환경적 특성과 지하비축기지라는 시설적 특성으로 인해 단순하지 않은 해수의 유입이 예상되는 곳으로 다양한 접근 방법을 갖고 연구가

진행되었다. Cl^-/Br^-의 비율, 주요 이온들의 주성분 분석, 안정동위원소 자료들로부터 나온 결과들과 현장의 수리지질학적 특성을 종합하여 비축기지 삼출수의 염분 기원과 염화 정도를 분석하였다.

주요어: 지하수 수질, 모델링, 확률적 포획권, 회귀 분석, 주성분 분석, 안정동위 원소, 전기 비저항 탐사, 이미지 유사성

감사의 글

이 논문이 완성되기 까지 도움을 주신 모든 분들께 진심으로 감사 드립니다. 먼저 학위 기간 내내 믿음과 격려로 지도해주신 이강근 교수님께 감사 드립니다. 논문 심사 과정 중 아낌 없는 조건으로 도움을 주신 이인성 교수님, 김준모 교수님, 김규범 교수님, 현윤정 박사님께 감사의 뜻을 전합니다.

각자의 위치에서 늘 노력하는 모습으로 좋은 본보기가 되어 주시는 수리지구 환경 연구실의 여러 선배님들께도 감사의 인사 드립니다. 함께 연구실 생활을 하지 못했음에도 후배라는 이유로 관심과 격려를 아끼지 않는 마음에서 많은 것을 받고 배웁니다.

오랜 기간 동안 연구실 생활을 함께 해준 선후배, 동기 분들께도 특별한 감사를 드립니다. 저의 여러 부족함 점들을 참아주시고 채워주신 여러분들이 있었기에 연구실 생활을 할 수 있었습니다. 함께 한 것 만으로도 큰 힘이 되었습니다. 감사 드립니다.

마지막으로 있는 것 만으로도 힘이 되는 동생 건우와 언제나 믿음으로 지지해주시고 한결 같은 마음으로 기댈 곳이 되어 주신 사랑하는 부모님께 깊이 감사 드립니다.